Author Manuscript

Author Manuscript

Author Manuscript

Author Manuscript

HHS Public Access

Author manuscript

Biochemistry. Author manuscript; available in PMC 2020 December 30.

Published in final edited form as:

Biochemistry. 2020 June 30; 59(25): 2371–2385. doi:10.1021/acs.biochem.0c00293.

Human γS-crystallin copper binding helps buffer against aggregation caused by oxidative damage

Kyle W. Roskamp[†], **Sana Azim**[‡], **Günther Kassier**[‡], **Brenna-Norton Baker**[†,‡], **Marc A. Sprague-Piercy**[¶], **R. J. Dwyane Miller**[‡,§], **Rachel W. Martin**[†,¶]

[†]Department of Chemistry, University of California, Irvine, CA 92697-2025, USA

[‡]Max Planck Institute for the Structure and Dynamics of Matter, Center for Free Electron Laser Science, Luruper Chaussee 149, 22761, Hamburg, Germany.

[¶]Department of Molecular Biology and Biochemistry, University of California, Irvine, CA 92697-3900, USA

[§]Departments of Chemistry and Physics, University of Toronto, 80 St. George Street, Toronto, M5S 3H6 Canada

Abstract

Divalent metal cations can play a role in protein aggregation diseases, including cataract. Here we compare the aggregation of human γS-crystallin, a key structural protein of the eye lens, via mutagenesis, UV light damage, and the addition of metal ions. All three aggregation pathways result in globular, amorphous-looking structures that do not elongate into fibers. We also investigate the molecular mechanism underlying copper (II)-induced aggregation. This work was motivated by the observation that zinc (II)-induced aggregation of γS-crystallin is driven by intermolecular bridging of solvent-accessible cysteine residues, while in contrast, copper (II)-induced aggregation of this protein is exacerbated by the removal of solvent-accessible cysteines via mutation. Here we find that copper (II)-induced aggregation results from a complex mechanism involving multiple interactions with the protein. The initial protein-metal interactions result in the reduction of Cu(II) to Cu(I) with concomitant oxidation of γS-crystallin. In addition to the intermolecular disulfides that represent a starting point for aggregation, intramolecular disulfides also occur the cysteine loop, a region of the N-terminal domain that was previously found to mediate the early stages of cataract formation. This previously unobserved ability of γS-crystallin to transfer disulfides intramolecularly suggests that it may serve as an oxidation sink for the lens after glutathione levels have become depleted during aging. γS-crystallin thus serves as

rwmartin@uci.edu.

Accession Codes

Human γS-crystallin - Uniprot: CRYGS_HUMAN, PDB ID: 2M3T, 6FD8

Mus musculus (mouse) γS-crystallin - PDB ID: 6MY8

Supplementary Information: Additional TEM images and characterization data for the γS-crystallin aggregates. FTIR spectra, SEC and SDS-PAGE data, and mass spectrometry data. A figure showing potential ion-binding sites. Tabulated literature data for the cysteine content of human crystallin proteins.

Conflict of interest

The authors declare that they have no conflict of interest.

Author Manuscript Author Manuscript Author Manuscript Author Manuscript

the last line of defense against oxidation in the eye lens, a result that underscores the chemical functionality of this protein, which is generally considered to play a purely structural role.

Introduction

The eye lens is a unique organ due to its optical transparency and minimal metabolic activity. Lens tissue is characterized by high protein concentrations, ranging to upwards of 400 mg/mL in humans.[1] 90 % of lens proteins belong to the α-, β-, and γ-crystallin families. The α-crystallins are small heat-shock proteins that function as holdase chaperones, whereas the β- and γ-crystallins are structural proteins evolved for high refractivity and fluorescence quenching. Both β- and γ-crystallins contain two domains connected via a linker sequence and held tightly together by a hydrophobic interface. Each domain contains a double Greekkey motif in which two sets of four antiparallel β-strands create a β-sandwich structure. Even small disruptions to this highly stable structure can lead to stabilization of aggregation-prone intermediates, and ultimately to aggregation[2–4]

The lens crystallins are extremely long lived proteins (ELLPs) that face considerable challenges to their stability and solubility. Under a thin exterior layer of epithelial cells, the lens is made of elongated fiber cells that enucleate and lose their organelles during maturation in order to eliminate light scattering. This process removes the cellular machinery necessary for protein turnover, thus, lens proteins are not replaced during an organism's lifetime. The lens is routinely exposed to ultraviolet radiation, which can cause structural damage, and the α-crystallins that help maintain solubility can only solubilize damaged structural crystallins but are unable to refold them.[5,6] Consequently, the β- and γ-crystallins have evolved efficient fluorescence quenching mechanisms through conserved structural features and FRET interactions between the buried tryptophans in each domain.[7–10] The aggregation-promoting effect of mutating these Trp residues to Phe is especially strong for those that are most strongly quenched, consistent with the photoprotective quenching requiring multiple Trp residues.[11] Trp residues are also susceptible to undergoing UV photochemistry, producing kynurenine, a small molecule that can act as a UV filter,[12] but can also covalently attach to crystallin proteins, exacerbating oxidative damage.[13] The modified Trp residue left behind upon kynurenine formation can also promote aggregation, as demonstrated by investigating the properties of point variants mimicking this modification.[14]

The lens environment also contains high levels of glutathione and other antioxidants that serve as redox buffers.[15] Despite these adaptation, deleterious post-translational modifications (PTMs) do accumulate over time.[16,17] An array of PTMs are observed in both the soluble and insoluble fractions of aged lenses, and appear to promote protein aggregation, leading to age-related cataract formation.[18,19] In many cases, the molecular-level details of how PTMs exacerbate aggregation remain unclear. Two modifications of significant interest are deamidation and oxidation. Deamidation, the most commonly observed modification[17,20] can lead to altered dynamics and reduced stability,[21,22] and may occur in parallel with racemization or isomerization.[23,24] Oxidation is arguably the second most common PTM, and is thought to accumulate with age as lens antioxidant levels

Author Manuscript Author Manuscript Author Manuscript Author Manuscript

decrease. Mass spectrometric identification of aged lens γ-crystallins has given evidence for oxidative damage to numerous residues, focally methionine, histidine, tryptophan and cysteine.[16,25] Although reactive oxygen species (ROS) formation in the lens can result from regular exposure to UVA[26] (0.116 – 0.99 mW cm^{-1}) and UVB (1.2×10^{-4} – 4.4×10^{-4} mW cm^{-1}) radiation27[1], their formation may also be catalyzed by metal ions found in the lens.

Copper and zinc ions in the lens serve as cofactors for the chaperone α-crystallins, but are released upon substrate binding.[28] Whether this release contributes to a negative feedback cycle is currently unknown; however, elevated copper levels have been reported in cataract lenses.[29–31] Increased copper concentration in the lens may also be a feature of diabetes[32] and smoking,[33] but this is difficult to measure directly. Although the concentration of lens Zn^{2+} is several times higher than Cu^{2+},[34] copper ions readily produce ROS and induce γ-crystallin aggregation at lower equivalencies.[35] The molecular mechanisms of aggregation due to copper ions and associated ROS are poorly understood, but are potentially relevant in other protein aggregation diseases such as Alzheimer's, Parkinson's, and Huntington's.[36,37] The specific interactions with copper ions depend on the structure and function of the protein. Some disease-related proteins like α-synuclein,[38,39] β-amyloid,[40,41] and ubiquitin[42] aggregate in the presence of copper ions, whereas in prion[43] and tau,[44] aggregation is inhibited.

γS-crystallin is highly expressed in the lens epithelial and cortical fiber cells,[45] while γC and γD – the other highly expressed γ-crystallins – are primarily concentrated in the lens nucleus.[46,47] Because copper ions are relatively evenly distributed throughout the lens,[48] their interactions with all of the structural crystallins are physiologically relevant. We previously reported that divalent cations of zinc, nickel, and cobalt drive γS-crystallin aggregation through intermolecular bridging via cysteines, whereas copper-induced aggregation occurs even in the absence of solvent-accessible cysteines.[35] Solution-state nuclear magnetic resonance (NMR) studies of γD-crystallin suggest that the strongest copper interactions occur at sites with at least two proximal cysteines or histidines.[49] Here we focus on investigating the mechanistic pathways of copper-mediated aggregation of γS-crystallin, which contains a unique cysteine tetrad.[50]

Three of the cysteines, C23, C25, and C27, are solvent-accessible and within disulfide bonding distance of one another. The fourth cysteine, C83, is located on an adjacent β-strand, within hydrogen-bonding distance of C23 and C27. Although no function is yet known for this tetrad, other γ-crystallins have been observed to have an oxidoreductase-like property where intramolecular disulfides are transferred between proteins.[51] It has been proposed that continual transfers amongst the highly concentrated γ-crystallins may act as a final redox buffer. A diffusion barrier at the boundary between the lens nucleus and cortex impedes gluathione transport into the nucleus,[52] raising the possibility that proteins in the cortex remain reduced longer. However, given the low protein turnover in this environment, oxidation and associated post-translational modifications are inevitable consequences of aging for all of the lens proteins. Since the cysteines of γS are the most solvent-exposed and

[1]Ranges represent 2% – 17% impingement of solar radiation in summer at 40°N applied to data for UVB 295 – 315 nm) and UVA (315 – 400 nm) light.

Author Manuscript Author Manuscript Author Manuscript Author Manuscript

highest density cysteines in the γ-crystallin, they may serve as a sink for any disulfide transfer mechanism in the lens.

In order to better understand the aggregation pathways of γS-crystallin, we have investigated copper (II)-mediated aggregation alongside UV-induced aggregation and point mutations implicated in hereditary cataract. Although the morphologies of all γS-crystallin aggregates examined here are indistinguishable, their relative hydrophobic surface exposures vary. Copper-induced aggregation itself is buffered by the solvent-accessible cysteine residues and is partly reversible through the chelation of copper ions. Aggregation of γS-crystallin can be attributed to copper ion binding and oxidation, which further results in structural changes in the protein. Unsurprisingly, the process of Cu^{2+}-induced aggregation involves several mechanisms, however, the ability of γS to limit oxidative damage further suggests that the lens γ-crystallins have evolved to act as a final redox buffer in the lens.

Materials and methods

Protein Expression and Purification

The human γS-crystallin variants γS-G18V, γS-D26G, and γS-V42M, and γS-C23S-C25S-C27S-C115S (γS-C_0) were made using site-directed mutagenesis of the wild-type (γS-WT) construct containing an N-terminal 6× His tag and a TEV cleavage sequence (ENLFQG), which leaves a glycine in place of the initiator methionine. The genes encoding each protein were cloned into a pET28a(+) vector (Novagen, Darmstadt, Germany) and overexpressed in a Rosetta *E. coli* cell line (DE3) using Studier's autoinduction protocol.[53] Cell pellets were collected via centrifugation at 4,000 rpm for 30 minutes, resuspended, lysed via sonication, and respun at 14,000 rpm for 60 minutes. Each protein was purified via nickel affinity chromatography, digestion with TEV protease (produced in-house), subsequent nickel affinity chromatography to remove the His tag, and finally, two separate size exclusion chromatography (SEC) runs on a GE Superdex 75 10/300 (GE Healthcare, Pittsburgh, PA) to ensure pure monomeric protein. All samples were dialyzed into 10 mM HEPES, 50 mM NaCl, pH 7 unless otherwise stated. Prior to measurement, proteins were reduced using 5 mM fresh dithiothreitol (DTT) and dialyzed. Analytical size exclusion of copper-treated samples were measured using a GE Superdex 75 Increase 10/300 GL (GE Healthcare, Pittsburgh, PA).

UV-A Induced Aggregation

Protein solutions at 6 mg/mL (2.5 mL) or 100 mg/mL (1.5 mL) were irradiated with 355 nm light generated using a 10 Hz Nd:YAG laser (Continuum Surelite II; Surelite, San Jose, CA, USA) coupled to a Surelite Separation Package (SSP) 2A (Surelite) to change the pump laser wavelength (1064 nm) via third harmonic generation (laser flux was 29 mJ/cm^2 at 10 Hz). The solutions were continuously stirred and kept between 22 °C and 24 °C using a Quantum Northwest Luma 40/Eclipse with a Peltier element and recirculator (Quantum Northwest Inc., Liberty Lake, WA, USA). Samples were irradiated for 180 minutes consistent with our previous investigation of UVA-irradiated crystallins.[54]

Author Manuscript Author Manuscript Author Manuscript Author Manuscript

UV-B Induced Aggregation

Aggregation of 6 mg/mL or 100 mg/mL γS-crystallins via 278 nm UVB radiation was accomplished using two 70mW light emitting diodes (LEUVA66H70HF00, Seoul, Korea) at 5 mm distances (120 degree view angle) yielding a mean power density of 58 mW/cm^2. Samples used for TEM and FTIR measurements were irradiated for 30 minutes as preliminary tests showed that this was the shortest exposure time that provided a sufficient amount of aggregated material. TEM images of samples measured at all time points showed morphologically similar aggregates.

Absorbance

Resolubilization assays were performed by adding 200 μL of $CuCl_2$ stock solutions to 200 μL of protein to achieve final solutions of 50 μM protein varying molar equivalents of $CuCl_2$. Samples were incubated at 25 °C for 8 hours and then left at 4 °C overnight prior to measurement. Samples were then spun at 6000 rpm for 20 minutes, and the supernatant was carefully removed so as to not disrupt any pelleted aggregates. Aggregates were resuspended in 400 uL of buffer with 10 mM ethylenediaminetetraacetic acid (EDTA), vortexed, incubated at 37 °C for 30 minutes, sonicated for 15 minutes, and respun at 6000 rpm. This procedure was then repeated with the addition of dithiothreitol (DTT) for a final concentration of 5 mM (2 μL of 1 M DTT). EDTA and DTT treatments were also applied to the initial soluble samples following measurements. Absorbances were measured using a NanoDrop2000. Three samples were prepared for each concentration and each samples was measured in triplicate. Final absorbance values were corrected for dilution.

Tryptophan Fluorescence

All fluorescence measurements were performed using a Varian Cary Eclipse fluorescence spectrophotometer with 5 μM concentrations. The intrinsic tryptophan fluorescence spectra of protein samples was measured via excitation at 295 nm and emission spectra collected from 310 nm to 400 nm.

ANS Fluorescence

Fluorescence of 8-Anilinonaphthalene-1-sulfonic acid (ANS) was used as an indicator for hydrophobic surface exposure. Samples were prepared at final concentration of 50 μM with 750 μM ANS (based on previous work[55]) and allowed to incubate at room temperature for one hour. Fluorescence spectra were measured from 450 nm to 600 nm with an excitation of 390 nm, using 20 nm slit widths.

Isothermal Titration Calorimetry (ITC)

ITC measurements of copper ion binding were performed using a MicroCal PEAQ-ITC (Malvern Instruments, Northampton, MA, USA). Two hundred μL of freshly reduced γS-WT (135 μM) and γS-C_0 were titrated with 4 mM of $CuCl_2$ at 25 °C. Injections were made every 225 seconds, with 25 titrations in total. The ITC data were initially analyzed using MicroCal PEAQ-ITC Analysis Software. The reported parameters are the mean and standard deviation of three independent trials. Based on the similarity of the transition metal FRET (tmFRET) and initial ITC binding data, the binding parameters for γS-C_0 were determined

Author Manuscript Author Manuscript Author Manuscript Author Manuscript

first using a single binding site model. The number of sites was constrained between 0.25 and 1.5, and the binding constant was limited to 1×10^{-8} based on preliminary model fitting performed in R[56] using the 'Ritc' package.[57] For γS-WT, the data was fit to a two site binding model, using the γS-C_0 parameters and initial values for the second γS-WT binding event.

Fluorescence Quenching

Fluorescence quenching of γS-WT and γS-C_0 was done by adding 2 μL of 125 μM $CuCl_2$ to 500 μL of 5 μM protein yielding 0.1 molar equivalent steps. Following $CuCl_2$ addition, the sample was gently shaken and then allowed to equilibrate for 20 seconds prior to measurement. The emission spectra were measured from 320 nm to 360 nm using 295 nm excitation to minimize tyrosine and phenylalanine absorbance. The Stern-Volmer binding constants were calculated assuming static quenching using the equation $F_0/F = 1 + K_{SV}[Q]$, where F_0/F is the ratio of the initial fluorescence intensity at 330 nm, K_{SV} is the Stern-Volmer binding constant, and [Q] is the concentration of $CuCl_2$. For γS-WT, two separate models were generated to fit the data from amounts less than and greater than 0.5 equivalents of $CuCl_2$, as a clear difference in quenching is observed. The K_{SV} of γS-C_0 was calculated through ~1.5 molar equivalents. After this point the behavior F_0/F data exhibits logarithmic behavior, consistent with binding saturation in fluorescence quenching studies of proteins containing buried tryptophans.[58,59] Further, after 1.5 molar equivalents, linear regression models maintain an r-squared above 0.99. No significant changes were observed in the K_{SV} of either protein when calculated for all measured emission wavelengths, therefore, the data presented uses the 330 nm emission intensities.

Fourier-transform infrared spectroscopy (FTIR)

Aggregates of γS-G18V, γS-D26G, and γS-V42M were collected from samples stored at 5 mg/mL at 4 °C for several weeks. All aggregates and soluble protein were separated via centrifugation and lyophilized. Samples were then resuspended in D_2O for 24 hrs and lyophilized again. Measurements of all powders were made using a Jasco FT/IR-4700-ATR-PRO ONE (JASCO, Easton, MD) over the 400–4000 cm^{-1} range with 4 cm^{-1} resolution. Data from 1700 cm^{-1} to 1475 cm^{-1} normalized to peak amide I band absorbance.

Liquid Chromatography - Mass Spectrometry (LC-MS)

In-line separation of protein and peptide fragments and subsequent mass spectrometry measurements were performed on a Waters Xevo XS-QTOF using a Waters BEH C4 50mm column with a 0.3 mL/min flow rate. Protein samples were diluted 10:1 in 0.1% formic acid and separated using a gradient where solvent A = 100% 0.1% formic acid in water and solvent B = acetonitrile. The gradient started at 3% solvent B for one minute followed by a linear ramp to 27% B over 5 minutes. Peptide samples were generated from aggregates produced by incubating freshly reduced γS-WT with 1 equivalent of $CuCl_2$ for 24 hours at room temperature. Protein samples of 1 mL at 200 μM were incubated overnight with 3 μg of trypsin at 37 °C. Samples were diluted and measured in an identical manner to protein samples except for an extended separation time of 25 minutes. Reduced peptide samples were treated with fresh DTT for 5 minutes at room temperature prior measurement. All data analysis was performed using BioPharmaLynx software for fragment identification. Peptide

Author Manuscript Author Manuscript Author Manuscript Author Manuscript

fragment identities were confirmed via direct inspection of the raw data and isotope pattern analysis. Over several replicates the sequence coverage varied between 70% and 85%. For each of the cysteines, at least one fragment was identified. The presence of disulfide bonded fragments was confirmed via the disappearance of identified peaks in reduced samples.

SDS-PAGE

The γS-WT (200 μL total volume, 150 μM) samples were aggregated using 0.1, 0.2, 0.4, 0.6, 0.8, 1, 1.5, 2, 3, or 5 equivalents of $CuCl_2$ at 25 °C for 4 hours and then left at 4 °C overnight. The samples were then centrifuged, and the supernatant was removed without disturbing the pellet. Prior to loading, 10 μL of protein was mixed with 10μ of loading dye (62.5 mM Tris-HCl, 2% sodium dodecyl sulfate, 25% glycerol, 0.01% bromophenyl blue, pH 6.8), 1 μL 2-mercaptoethanol, 1 μ of EDTA (final concentration 1 mM), and heated at 70 °C for 90 seconds. Samples were run on 12% Mini-Protean TGX gel at 115 V for 85 minutes and stained using Coomassie blue dye. Each gel was run at least twice to verify reproducibility.

Analytical Size Exclusion Chromatography (SEC)

Samples of freshly reduced γS-crystallins were mixed with $CuCl_2$ in 1:1 ratios resulting in a final sample at 50 μM with 0, 0.25, 0.5, 0.75, or 1 equivalent of $CuCl_2$. The samples were allowed to incubate at room temperature overnight and were subsequently stored at 4 °C until use. Prior to measurement, samples were treated with 100-fold excess of EDTA. For re-reduced samples, subsequent treatment with fresh DTT followed by incubation at 37 °C for 30 minutes was also performed. Prior to measurement, samples were passed through a 0.45 μm filter to eliminate potential aggregates. The separation of soluble aggregated species was achieved by loading 500 μL of sample onto a Superdex 75 Increase 10/300 GL column. The sample and column temperature were maintained at 4 °C and the flow rate was 0.8 mL/min. Elution was monitored via the absorbance at 280 nm.

Transmission electron microscopy

The morphology of the γS-crystallin aggregates formed on exposure to acidic buffer, UV irradiation, or metal ion treatment were investigated by transmission electron microscopy (TEM). Samples were prepared at concentrations of 6 mg/mL or 100 mg/mL and used without further dilution. Negatively stained samples for TEM were prepared on commercial carbon-coated 400 mesh copper grids (Plano GmbH, Wetzlar, Germany). The grids were made hydrophilic by glow discharge treatment, whereupon 2 μl of sample solution was applied and allowed to soak for 45 seconds before blotting. The grids were then rinsed twice with 50 μL deionized water, followed by blotting. Negative staining was performed by applying 4 μl of a 1 percent uranyl acetate solution, followed by immediate blotting. Application of 4 μl of uranyl acetate was then repeated, this time being allowed to soak for 20 seconds before a final blotting step. TEM micrographs were then recorded in a JEOL JEM 2100 instrument with an accelerating voltage setting of 120 kV.

Author Manuscript Author Manuscript Author Manuscript Author Manuscript

Results and Discussion

Amorphous-looking aggregates are formed from point variant, UV-irradiated, and copper-damaged γS-crystallins

Unlike the amyloid fibrils central to many protein deposition diseases, crystallin aggregates are frequently characterized as amorphous-looking, although fibrillization of lens crystallins is readily induced *in vitro* using extreme pH conditions. Herein, we have investigated the aggregation of wild-type human γS-crystallin(γS-WT) resulting from treatment with copper (II), and compared the aggregates to those resulting from known cataractous point mutations and UV irradiation. Transmission electron microscopy (TEM) was used to image aggregates of γS-G18V, γS-D26G, and γS-V42M that formed after being stored at 4 °C for over one month (Figure 1A–C), which we will refer to as “native aggregates”. For each variant, the native aggregates have a granular appearance and are composed of smaller globular particles roughly 25 nm in diameter on average (SI Figure S1), similar to those we have previously observed for UV-aggregated γS-crystallin samples.[54] The clustering of smaller, component aggregates observable in each case is similar to that observed for the γD-P23T point variant in prior studies by other groups.[60,61] Furthermore, the morphological similarity of aggregates observed here is striking, as the D26G variant – in which only a surface salt bridge is lost[62] – is qualitatively different from G18V and V42M, both of which cause more substantial structural changes to the N-terminal domain.[63,64]

TEM micrographs of γS-crystallin were collected following UVA and UVB irradiation (Figure 1D–E). Although UVA and UVB can both catalyze ROS formation, the lower levels of UVB reaching the lens are effectively quenched due to their absorption by aromatic residues, particularly the four strongly-conserved tryptophans.[8] Irradiation over both wavelength ranges produces aggregates that are similar in size to the point variant aggregates, and similarly appear to lack any well-defined morphology that would be consistent with an ordered, repeating structure. To ensure that the UV aggregates formed were representative, we varied the concentration and irradiation times of the samples to assess potential differences. In all cases, once formed, the size and morphology of the observed aggregates did not exhibit any notable differences (SI Figures S2–S3). Likewise, photodamaged point variants also show distinct, small component aggregates similar in size to native aggregates (SI Figure S4).

As observed for point variants and UV irradiated samples, copper (II)-induced aggregates lacked distinctive repetitive structure (Figure 1F), consistent with observations of copper (II)-induced aggregates of γD-crystallin.[49] In order to test for differences that would enable investigation of specific aggregation pathways, we probed the structure of the resulting aggregates via FTIR. In FTIR of proteins, the amide I band largely results from C=O stretching vibration, while the amide II band is mainly composed of the N-H bending vibration and C-N stretching vibration.[65] The amide absorption frequencies of protein secondary structures differ from one another; therefore one can infer structural differences by comparing the amide I and II bands. Between the soluble and aggregated variant γS-crystallins, minimal differences were observed in the amide I band line shape, suggesting that the overall β-sheet structure is retained for each of the solid aggregates (SI Figure S5).

Author Manuscript Author Manuscript Author Manuscript Author Manuscript

Likewise, the changes observed following UVB irradiation or treatment with copper ions are also minimal. Interestingly, the absorption of the amide I mode relative to amide II decreases for all aggregates, as well as the soluble UVB and copper salt-treated species. The extent to which the amide I and amide II peaks are modified for the UVB-treated samples differs noticeably from those observed in the one previous study of structural changes in UV-treated γB-crystallin.[66] We hypothesize that the smaller changes we observe are the result of minor conformational changes; however, specific structural modifications cannot be readily determined via FTIR alone, making this a promising direction for future high-resolution structural studies.

We next turned to potential changes in hydrophobic surface exposure in order to better understand the effect of copper treatment. Cataract-causing point mutations serve as convenient references, as increased hydrophobic surface exposure can result from mutations within the hydrophobic core[67,68] or on the protein surface,[55,69] although not all aggregation-prone variants exhibit increased hydrophobic surface exposure.[62] We assessed differences in exposed hydrophobic surface of γS-crystallin following copper and UVB treatment using ANS, a small molecule probe that fluoresces strongly when coordinated to a protein through a combination of electrostatic and hydrophobic interactions.[70] The soluble fraction of γS-WT that remains after $CuCL_2$ treatment has a similar ANS fluorescence spectrum to that of γS-D26G (Figure 2), for which no structural changes are known. Both spectra have slightly greater fluorescence maxima than that of untreated γS-WT. In contrast, the two point variants with known increases in hydrophobic surface exposure, γS-G18V and γS-V42M, show considerable increases in ANS fluorescence intensity upon binding the dye.

Interestingly, UVB-exposed γS-WT exhibits the greatest increase in ANS fluorescence, with an intensity more than double that of γS-V42M. UV-induced damage of γ-crystallins primarily occurs via tryptophan, cystine, and methionine oxidation,[71] and is able to disrupt the hydrophobic core of the protein, as all four tryptophans are buried and integral to the Greek key domain structure. In contrast, given the absence of large-scale unfolding, we hypothesize that copper-mediated damage is limited to binding or oxidation of surface residues. In contrast, given the absence of large-scale unfolding, we hypothesize that copper-mediated damage is limited to binding or oxidation of surface residues. In a prior study, we observed small amounts of methionine and cysteine oxidation at high $CuCl_2$ concentration, which was part of the rationale for further investigation of the mechanism.[35] Our results indicate that the remaining soluble γS-WT following UVB and copper treatment differ in their extent of hydrophobic surface exposure, with aggregation likely occurring through different pathways. We previously observed that γS-WT aggregates from copper treatment contain PTMs, albeit at low levels.[35] Taken together, these data indicate that the binding interactions of copper and γS-crystallin promote the onset of aggregation.

Copper induces aggregation via multiple mechanisms

Recently, divalent cations of transition metals such as copper,[49,72] zinc,[35,73] and mercury[74] have been shown to facilitate γ-crystallin aggregation. We previously observed that γS-crystallin samples treated with Zn^{2+}, Ni^{2+}, and Co^{2+} aggregate through an intermolecular bridging type mechanism, which becomes negligible upon the mutation of all solvent-

Author Manuscript Author Manuscript Author Manuscript Author Manuscript

accessible cysteines to serines. Surprisingly, removing these cysteines accelerated copper-induced aggregation.[35] In order to systematically evaluate the effect of copper ions, we began by investigating the aggregation of γS-WT and the engineered γS-C_0 variant, in which all four solvent accessible cysteines (C23, C25, C27, and C115) were mutated to serine. Consistent with our previous results, γS-WT aggregates to a lesser total extent than γS-C_0 when treated with varying equivalents of $CuCl_2$ (Figure 3A–B). In order to quantify aggregation-promoting factors, we treated insoluble copper-induced aggregates with excess EDTA (10 mM) to recover protein precipitated through intermolecular bridging. Both proteins show comparable amounts of recovery relative to the amount of insoluble aggregate formed (Figure 3C). Subsequently, we resuspended the remaining aggregates in the presence of DTT (5 mM) in order to disrupt potential disulfide crosslinks contributing to aggregation (Figure 3D). Unexpectedly, we observed apparent resolubilization of both proteins, although small aggregates may still be present. Although intermolecular disulfides or non-native disulfide trapped folds may play a role in causing aggregation, we suspected that the copper oxidation state may explain the observed behavior. EDTA is an effective Cu(II) chelator (K_d of $10^{-18.8}$ M),[75] however, its ability to abstract Cu(I) is more limited. In comparison, DTT binds Cu(II) strongly and Cu(I) less so,[76,77] and is capable of generating Cu(I) from Cu(II). Therefore, DTT resolubilization may proceed via coordination of bound Cu(I), or by reduction of tightly bound Cu(II) to Cu(I), resulting in more weakly bound ion. Alternatively, protein-bound copper may result in steric shielding, limiting the EDTA to fewer accessible coordination sites, but still allowing for bidentate binding by DTT. In each case, the ability of a second chelating agent to resolubilize aggregates following EDTA treatment suggests that copper ion-induced aggregation occurs though more than one mechanism and may involve binding to at least two sites. In addition to intermolecular bridging and intermolecular disulfide bonding, we hypothesized that the tightly bound copper ions may induce local structural modifications leading to additional aggregation pathways.

Structural changes to the resolubilized proteins were investigated via fluorescence and circular dichroism (CD) spectroscopy. The tryptophan fluorescence of γ-crystallin is a sensitive measure of conformational changes observable through reduced FRET efficiency and red-shifting due to increased polarity in the local tryptophan environment.[7,9] For both proteins, the EDTA-resolubilized species exhibit the greatest extent of red shifting of the fluorescence signal, indicating the most unfolding. The extent of unfolding for all copper-treated species was assessed via the 355/325 nm fluorescence intensity ratio.[78,79] This method is preferable to measuring at a single frequency, as it provides a quantitative measure of unfolding, which is particularly useful for detecting incomplete unfolding, as in the case where one domain unfolds before the other. The ratio is also useful for comparing samples where different degrees of partial unfolding have occurred.

The fluorescence ratios of EDTA-resolubilized γS-WT and γS-C_0 increased from 0.57 to 0.78 and from 0.59 to 0.96, respectively. The 355/325 nm fluorescence ratios around ~ 0.9 are indicative of partial domain unfolding. Similar fluorescence ratios have been reported for the chemical denaturation of γS-G18V,[80] γS-S39C,[3] γS-V42M[67] and γD-V75D.[81] NMR and SAXS of chemically denatured γD-V75D have shown the CTD remains folded while the NTD becomes unfolded.[82] In the case of copper-induced unfolding, we hypothesize that

Author Manuscript Author Manuscript Author Manuscript Author Manuscript

the NTD similarly unfolds. The three NTD cysteines are significantly more solvent-exposed than the lone CTD cysteine and thus likely to interact with copper, leading to structural modifications. Interestingly, the fluorescence ratios for both DTT-resolubilized proteins suggest negligible unfolding, further evidencing that multiple mechanisms are involved in copper-induced aggregation.

The CD spectra were also measured for all copper-treated species in order to compare to the fluorescence ratio unfolding results. For γS-WT, the CD spectrum exhibits a minimum at 218 nm, indicative of high β-sheet character, consistent with the solution-state NMR structure.[64] Minimal structural changes were evidenced in the soluble γS-WT. For soluble γS-C_0, the CD absorbance is low relative to the untreated sample and shows an increased absorbance around 205 nm. This result is likely from a minor reduction in the β-sheet character with a concomitant increase in random coil character, but is more dramatic than the change observed in the fluorescence ratio. In comparison, the CD spectra for the both DTT-resolubilized species exhibit minimal differences relative to the untreated protein; indicating only minor structural differences, while the EDTA-resolubilized species of both proteins indicate considerable structural changes. For γS-C_0, the minima near 200 nm and from 212 to 218 nm, indicating a considerable reduction in β-sheet character with no changes in the α-helix content and an increase in random coil content. The CD spectra of EDTA-resolubilized γS-WT is similar, but lacks the minima near 200 nm, suggesting the structural changes are not nearly as severe as those in C_0. These results are consistent with the observed fluorescence ratio data, indicating the extent of unfolding in the EDTA- and DTT-resolubilized species differ considerably. Further, these observations support a function for the NTD cysteines in preventing the copper-induced unfolding.

The cysteine loop in γS-WT is responsible for high-affinity copper binding

While analyzing the γS-crystallin fluorescence data, we suspected that the reduced intensity of the copper-treated species resulted from transition metal FRET (tmFRET) interactions with bound copper. Although no metal-binding site has previously been identified for human γS-crystallin, several transition metals are able to drive intermolecular bridging via the cysteine loop.[35] As copper appeared to bind γS at two or more sites, we presumed one to be the cysteine loop. TmFRET interactions can be used to calculate binding constants from fluorescence quenching when the interactions occur between the metal and fluorophore. The observed tmFRET from yS-crystallin is complicated by the presence of four buried tryptophans; therefore, we measured the quenching constants for γS-WT and γS-C_0 to probe how the solvent-accessible cysteines affect the copper ion binding.

Stern-Volmer plots and binding constants (K_{SV}) were generated from fluorescence measurements of $CuCl_2$ titrations (Figure 5A). In the Stern-Volmer plot for γS-WT, the ratio of the initial to $CuCl_2$-treated fluorescence intensity – used to measure the extent of quenching – sharply changes at 0.5 equivalents of $CuCl_2$. Two K_{SV} were calculated around this point, and show that the strong initial binding of γS-WT ($K_{SV1} = 12.1 \times 10^3$) is reduced over two fold in the second regime ($K_{SV2} = 4.5 \times 10^3$) (Table 1). The K_{SV2} of γS-WT is similar to the K_{SV1} of γS-C_0 (6.1×10^3). We posit that the second copper-binding event with γS-WT is equivalent to the γS-C_0 binding, and occurs following saturation of cysteine

Author Manuscript Author Manuscript Author Manuscript Author Manuscript

loop. Further, the binding and subsequent change in behavior at 0.5 copper equivalents for γS-WT is suspected to result from metal-bridging bridging between two cysteine loops.

Although tmFRET measurements give evidence for clear differences in copper binding by γS-WT and γS-C_0, we were unable to directly calculate binding constants from these data. Therefore, we used isothermal titration calorimetry (ITC) to probe the binding interactions (Figure 5B–D). Consistent with the tmFRET quenching, γS-WT exhibits two binding events and was analyzed using a two-site model. The first γS-WT binding event exhibits a higher affinity (K_d = 50 μM) than the second (K_d = 4 mM) (Table 2). For γS-C_0, the single binding event is similar in affinity to the second γS-WT event, further suggesting that the initial, high-affinity binding occurs at the cysteine loop.

In comparing known copper-binding sites to the cysteine loop, no similar structural motifs were observed, although several copper-transport proteins have similar local concentrations of cysteine residues. The binding sites of these metalloproteins coordinate to Cu(I) with remarkable affinity – up to 10^{-21} M for CueR[83] – and primarily use linear bicysteinate coordination. We suspect that a similar binding mode may occur for γS-WT, as the C23-C25, C23-C27, and C25-C27 side chain sulfurs (minimized sidechain rotamer distances of 3.8 ± 0.5 Å, 3.1 ± 0.3 Å, and 4.3 ± 0.1 Å, respectively[64]) are sufficiently proximal in the 20 lowest energy NMR confirmations of the native protein. Predictions of Cu(I) binding to γS-WT generated using MIB[84,85] also highlight the cysteine loop as the most likely binding site (SI Figure S6).

The calculated binding constant of the first γS event is considerably weaker than characterized domains of Atx1,[86] HMA7,[87] WLN5,[76] and other metalloproteins employing cysteinate binding motifs. As shown for *Pseudomonas aeruginosa* azurin, the thermodynamics of strong Cu(I) and Cu(II) binding are obscured in ITC analysis by sidechain deprotonations and metal-buffer interactions.[88] For the γ-WT copper binding measured here, potential disulfide bond formation and other unknown interactions with the protein may also contribute to the observed binding thermodynamics. Given these considerations, we hypothesize that the affinity of the cysteine loop for Cu(I) may be higher than reported here.

Cation-mediated bridging and disulfide bonding are the primary modifications resulting from copper treatment of γS-crystallin

In order to determine whether the copper-induced structural changes observed at the protein level translate into any higher-order structure, we probed aggregate size distributions via analytical SEC. In order to probe the smallest component sizes of the γS-WT and γSC_0 species, all samples were treated with EDTA and DTT prior to separation. The SEC traces of soluble and DTT-resolubilized γS-C_0 are primarily monomeric (SI Figure S7). This result is consistent with the minimal structural changes observed via CD and fluorescence, and supports a copper-induced aggregation mechanism involving metal-bridged crosslinking with coordination to non-cysteine residues. Despite the predominance of monomeric species, soluble and DTT-resolubilized γS-WT, but not γS-C_0, also contain a dimeric peak. As intermolecular disulfides between γS-crystallin are readily reducible, it is plausible that the cysteines are responsible for this alternative dimerization. The 2:1 stoichiometry

Author Manuscript Author Manuscript Author Manuscript Author Manuscript

observed in the binding assay also suggests that copper-mediated dimerization via the cysteine loop may be responsible, however, alternate mechanisms such as covalent intermolecular bond, e.g. dityrosine,[89] also require further investigation.

The chromatograms of EDTA-resolubilized γS-WT and γS-C_0 show higher molecular-weight species than soluble and DTT-resolubilized samples. Notably, γS-C_0 contains a greater proportion of non-monomeric species. This results is consistent with the extent of structural changes, and suggest that the both the dimer and high molecular species may be attributable to structural modifications.

To further characterize the EDTA-resolubilized dimers of both proteins, the fractions were collected and subjected to intact protein LC-MS using a C4 UPLC column, as different γ-crystallin conformations have been shown to be separable[90] (Figure 6). Multiple peaks were present in both the γS-WT and γS-C_0 traces, allowing us to perform independent mass reconstructions. The major elution peak for both proteins corresponded to an unmodified protein mass. The major peak in both protein traces also contained an earlier-eluting shoulder with a m+17 mass, likely due to methionine sulfoxide or cysteine sulfenic acid formation, as methionine and cysteine oxidations have previously reported for γS-crystallin.[35]

The later-eluting chromatographic peak of γS-WT was split in two. Reconstruction of the earlier peak showed the parent mass and an m+164 species. The later half of the second peak exhibited masses of m+221 and m+327. Likewise, the second peak of γS-C_0 – which eluted at the same time as the later half of the second γS-WT peak – contained an m+221 peak as well as an m+329 peak. Although interactions with the column may alter the observed eluted species, the bulk of the eluted protein is copper-free and a minority of protein species have mass shifts indicating the presence of multiple copper ligands. Assuming bound copper and oxidation account for most if not all of the observed mass shifts, an m+221 species may result from three bound copper ions and two oxidations. Similarly, a m+331 mass shift resulting from five bound copper ions and a single oxidation is similar to the observed m +327 and m+329 mass shifts.

In order to investigate the contribution of disulfide bonding to copper-induced aggregation, we subjected copper-treated γS-WT peaks from analytical SEC separations to LC-MS using only EDTA, but not DTT, prior to chromatographic separation. At only 0.25 equivalents of $CuCl_2$, a variety of high molecular weight species are readily observable, and become more pronounced with increased concentration of $CuCl_2$ (Figure 7A). A substantial recovery of low molecular weight species is possible via DTT addition; however the splitting of the final elution peak that is lost at 1 equivalent of $CuCl_2$ is not recoverable.

Mass reconstructions were used to probe the cause of the splitting observed in the final peak of the analytical SEC chromatograms. Notably, the left and right halves of the final peak contain monomeric and dimeric species (Figure 7B). A −2 Da mass shift occurs in the monomeric species of both final peaks, while a −4 Da mass shift occurs in both peaks' dimeric species. The persistence of the −2 Da mass shift in the monomeric species suggests an intramolecular disulfide bond, while the elimination of the dimeric 2m-4 peak follow

Author Manuscript Author Manuscript Author Manuscript Author Manuscript

DTT treatment suggest the presence of an additional intermolecular disulfide bond. Copper oxidation has been shown to facilitate disulfide bond formation in other γ-crystallins previously,[49,72] and intramolecular disulfide bond formation via the cysteine loop in γS has also been reported.[91]

Mass shifts characteristic of mono- and dioxidation are also present, consistent with intact mass spectrometry of C4-separated dimeric species and previously reported digests.[35] The combination of oxidation and disulfide bond formation accounts for the observed m+14, m +30, and 2m+12 peaks (Figure 7C). The remaining m+75 and m+91 monomeric peaks are +61 Da greater from the m+14 and m+30 peaks, respectively. This mass difference is consistent with copper binding via bicysteinate coordination. Although it is low in relative abundance, the presence of a 2m+59 peak also suggests bicysteinate coordination may be responsible for metal-bridged dimerization of two γS-crystallins. This observation is in line with the ITC and tmFRET data changes at 0.5 copper equivalents. Dimerization via an interface Cu(I) ligand involving a two-coordinate cysteinate binding site has previously been observed in metalloproteins such as Cox 17,[92] Hah1,[93] yCCS,[94] and Atx1.[95]

Intramolecular disulfides are present in addition to bound copper

In order to further characterize intramolecular disulfide bond formation and metal-binding resulting from copper addition, we turned to native SDS-PAGE. Proteins that remain more compact through conformational trapping[96–98] have been observed to migrate faster through a gel than their native counterparts. Metal binding can also exert a similar effect, whereby the extent of protein unfolding is limited by the geometry of the bound metal.[99] Native SDS-PAGE of $CuCl_2$-treated γS-WT shows four closely-spaced bands in the monomeric molecular weight range (Figure 8). The smaller splitting observed between the top and bottom pairs is attributable to the formation of an intramolecular disulfide (SI Figures S8–S9), while the larger splitting of the band pairs results from copper binding. Notably, similar metal-gel shifts are also apparent for γD-crystallin when incubated with copper ions.[49,72]

As little as 0.1 equivalent of copper is required to observe intramolecular disulfide bond formation and copper binding. Overloaded SDS-PAGE gels indicate that a small population of dimeric species is also present (SI Figure S8C). At higher copper:protein ratio, increased amounts of dimer are present, as are gel-shifted dimer bands indicating copper-bound species. Notably absent are any high molecular-weight bands corresponding to large aggregates. Although they are sometimes observed via analytical SEC, intact mass reconstructions show no evidence of species larger than the dimers. In contrast, aggregates of γD-crystallin produced with equivalent amounts of copper do exhibit high molecular weight species, which are reducible.[49] The SDS-PAGE bands corresponding to copper-bound γS-WT and γS-C_0 are eliminated upon addition of EDTA (SI Figure S10). The intramolecular disulfide band of γS-WT, however, is not eliminated by either EDTA or DTT addition.

In order to narrow down the location of the intramolecular disulfide bond, trypsin digests were performed on freshly prepared γS-WT that was allowed to incubate with 1 equivalent of $CuCl_2$ for 24 hours. The resulting peptides were separated and analyzed via liquid chromatography tandem mass spectrometry. The only observable intramolecular disulfide

Author Manuscript Author Manuscript Author Manuscript Author Manuscript

occurred between a peptide fragment containing the cysteine loop and a fragment containing C83. The disulfide bond between the fragments was confirmed through elimination by DTT (RT, 5 mins) and isotope pattern analysis. Secondary fragmentation patterns also indicated that the fragments were disulfide bonded, but were insufficient for determining which cysteine was bonded to C83. The structure of the loop region between the second and third β-strands projects the C25 sidechain outward (77 % SASA[35]) away from the C83 residue, making this residue unlikely to form the observed intramolecular disulfide without considerable structural rearrangement.[64] A C23-C83 (PDBID 6MYG) intramolecular disulfide has been observed in the X-ray crystal structures of mouse γS-crystallins, while a C27-C83 is also plausible as the residues are adjacent to one another in the three-dimensional structure.

γS-crystallin oxidation may act as a buffer against other copper-induced aggregation mechanisms

Relative to the α- and β-crystallins, γ-crystallins contain high levels of cysteine (SI Table S2). At first glance, it appears paradoxical that a protein that is functionally required to maintain a soluble monomeric state over the lifetime of an organism is enriched in this reactive amino acid. However, high cysteine content can be partially rationalized by this residue's considerable contribution to to the protein's refractive index.[35,100] Despite this, the solvent exposure of several γ-crystallin cysteines, particularly those of cysteine loop, seems incongruent with the importance of resisting oxidation and disulfide bonding in healthy lenses. In aged and cataract lenses, such PTMs have indeed been reported.[16] For γS-crystallin specifically, deamidation and disulfide bonding are particularly common modifications in aged lenses[101,102] and in oxidized samples.[103]

Recently, oxidized γD-crystallin was shown to transfer an intramolecular disulfide bond to the variant γD-W42Q, leading to the hypothesis that intramolecular disulfide bond transfer between γ-crystallins may serve as a final redox buffer for the lens after glutathione depletion.[51] Intermolecular and intramolecular disulfides have also been observed in recent x-ray crystal structures of human and mouse γS-crystallin dimers.[91] Given the high level of solvent exposure of the cysteine loop of human γS, we advance the hypothesis that the tetrad of cysteines in γS acts as a potential oxidation sink of last resort in the lens cortex. Our findings suggest an intramolecular disulfide bond involving C83, which would enable an internal disulfide bond isomerization mechanism for γS (Figure 10). This idea follows from the observation that C83 is buried within γS behind three proximal cysteines. The low abundance of dimeric species across several assays, the observation that γS-crystallin samples stored at higher concentration for extended periods of time result in more intramolecular than intermolecular disulfides (SI Figure S9), and the previous observation of disulfide bond transfer between γD-crystallins supports the hypothesis that γS-crystallin is able to exchange intermolecular disulfide bonds for intramolecular ones in order to remain monomeric. Potential intramolecular disulfide bonds and Cu^{2+} binding sites are shown in Figure 11. Alternatively, an intermolecular disulfide could also function as a lock to prevent unfolding of the native structure, as is observed for the homologous disulfide bond in simulations of γ-D crystallin.[104]

Author Manuscript Author Manuscript Author Manuscript Author Manuscript

Further experiments are needed to determine the precise locations of intra- and intermolecular disulfide bonds. However, based on the results available so far, we propose a hypothesis in which the cysteine loop could play a role in oxidative buffering mechanism, suggesting a purpose for the solvent-accessible cysteines of γS-crystallin beyond their generic role in enhancing refractivity. The proposed ability of the protein to store a disulfide internally is of considerable import given the recent observation that αA-crystallin oxidation reduces stability, but enables transfer of a disulfide bond to a substrate protein.[105] Future work will be required to determine whether γS-crystallin can accept a disulfide bond from αA *in vivo* as part of a tradeoff between increased αA activity and modification of this structural lens protein.

Conclusion

In this study, we observe that the removal of the solvent-accessible cysteines via mutagenesis increases the susceptibility of γS-crystallin to copper-induced aggregation. The reversibility of copper binding to both γS-WT and γS-C_0 – which lacks solvent exposed cysteines – indicates that multiple binding sites are present, raising the possibility that the cysteine tetrad of γS buffers against further aggregation by coordinating to a copper ion. The greater retention in structure of aggregated and soluble γS-WT compared to γS-C_0 also strongly suggests that the cysteine residues are important in buffering unfolding mediated aggregation. Part of the copper-buffering capacity of γS-WT is tied to the formation of intramolecular disulfide bonds. The intramolecular disulfide observed involves the buried C83 residue, highlighting the ability of the protein to isomerize a disulfide and also participate in copper binding. The extent to which the intramolecular disulfide may act to alter protein stability is yet unknown. Further experiments will be necessary to determine the additional copper-binding site beyond the cysteine loop, and thus refine our understanding of the copper-mediated unfolding mechanisms contributing to aggregation.

Supplementary Material

Refer to Web version on PubMed Central for supplementary material.

Acknowledgement

The authors acknowledge Dmitry Fishman for assistance and management of optical instruments at the UCI Laser Spectroscopy Labs, Ben Katz and Felix Grun for extensive help with mass spec data analysis and management of the UCI Mass Spectrometry Facility, Friedjof Tellkamp, Hendrik Schikora and Martin Kollewe from the machine physics support group and Djordje Gitaric and Josef Gonschior from the technical staff of the Max Planck Institute for the Structure and Dynamics of Matter, Hamburg Germany for setting up the UV-B source. This work builds on discussions at the 2018 Crystallin Satellite Biophysical Society Meeting in San Francisco, and we are grateful to the participants for ideas and suggestions.

Funding

This work was supported by NIH grants 2R01EY021514 to R.W.M and 1R01EY025328 to R.W.M. and D.J. Tobias. K.W.R was supported by the NSF Training Grant DGE-1633631 and DMS-1361425 to R.W.M. and C.T. Butts. B.N.B. was supported by the NSF GRFP and the Fulbright Fellowship. M.A.S.P was supported by the HHMI Gilliam Fellowship.

R.J.D.M. acknowledges the Max Planck Society and the Excellence Cluster “The Hamburg Center for Ultrafast Imaging (CUI)-Structure, Dynamics and Control of Matter at the Atomic Scale” of the Deutsche Forschungsgemeinschaft (DFG). R.W.M and R.J.D.M. are CIFAR Fellows.

Author Manuscript Author Manuscript Author Manuscript Author Manuscript

References

(1). Fagerholm PP; Philipson BT; Lindström B Normal human lens - the distribution of protein. Experimental Eye Research 1981, 33, 615–620. [PubMed: 7318958]

(2). Serebryany E; King JA The $\beta\gamma$-crystallins: Native state stability and pathways to aggregation. Progress in Biophysics and Molecular Biology 2014, 115, 32–41. [PubMed: 24835736]

(3). Vendra VPR; Khan I; Chandani S; Muniyandi A; Balasubramanian D Gamma crystallins of the human eye lens. Biochimica et Biophysica Acta (BBA)-General Subjects 2016, 1860, 333–343. [PubMed: 26116913]

(4). Serebryany E; Razban R; Shakhnovich EI Conformational catalysis of cataract-associated aggregation by interacting intermediates in a human eye lens crystallin. arXiv 2019, arXiv:1904.03653.

(5). Horwitz J; Bova MP; Ding L-L; Haley DA; Stewart PL Lens α-crystallin: function and structure. Eye 1999, 13, 403–408. [PubMed: 10627817]

(6). Stengel F; Baldwin AJ; Painter AJ; Jaya N; Basha E; Kay LE; Vierling E; Robinson CV; Benesch JLP Quaternary dynamics and plasticity underlie small heat shock protein chaperone function. Proceedings of the National Academy of Sciences of the United States of America 2010, 107, 2007–2012. [PubMed: 20133845]

(7). Chen J; Flaugh SL; Callis PR; King J Mechanism of the highly efficient quenching of tryptophan fluorescence in human γD-crystallin. Biochemistry 2006, 45, 11552–11563. [PubMed: 16981715]

(8). Chen J; Toptygin D; Brand L; King J Mechanism of the efficient tryptophan fluorescence quenching in human γD-crystallin studied by time-resolved fluorescence. Biochemistry 2008, 47, 10705–10721. [PubMed: 18795792]

(9). Chen J; Callis PR; King J Mechanism of the very efficient quenching of tryptophan fluorescence in human γD-and γS-crystallins: the γ-crystallin fold may have evolved to protect tryptophan residues from ultraviolet photodamage. Biochemistry 2009, 48, 3708–3716. [PubMed: 19358562]

(10). King J; Henry IM; Kosinski-Collins M; Thol S; Serebryany E Buried tryptophans contributing to the high kinetic stability of the long-lived gamma crystallins and their oxidative damage opening the pathway to the aggregated state associated with cataracts. Biophysical Journal 2020, 118, 181A.

(11). Schafheimer N; King J Tryptophan cluster protects human γD-crystallin from ultraviolet radiation-induced photoaggregation in vitro. Photochemistry and Photobiology 2013, 89, 1106–1115. [PubMed: 23683003]

(12). Bova L; Wood A; Jamie J; Truscott R UV filter compounds in human lenses: The origin of 4-(2-amino-3-hydroxyphenyl)-4-oxobutanoic acid O-beta-D-glucoside. Invest. Ophthalmol. Visual Sci 1999, 40, 3237–3244. [PubMed: 10586948]

(13). Parker NR; Jamie JF; Davies RJ, Michael Jand Truscott Protein-bound kynurenine is a photosensitizer of oxidative damage. Free Radic. Biol. Med 2004, 37, 1479–1489. [PubMed: 15454288]

(14). Serebryany E; Takata T; Erickson E; Schafheimer N; Wang Y; King JA Aggregation of Trp>Glu point mutants of human γD-crystallin provides a model for hereditary or UV-induced cataract. Protein Science 2016, 25, 1115–1128. [PubMed: 26991007]

(15). Giblin FJ Glutathione: a vital lens antioxidant. Journal of Ocular Pharmacology and Therapeutics 2000, 16, 121–135. [PubMed: 10803423]

(16). Hains PG; Truscott RJ Post-translational modifications in the nuclear region of young, aged, and cataract human lenses. Journal of Proteome Research 2007, 6, 3935–3943. [PubMed: 17824632]

(17). Wilmarth P; Tanner S; Dasari S; Nagalla S; Riviere M; Bafna V; Pevzner P; David L Age-related changes in human crystallins determined from comparative analysis of post-translational modifications in young and aged lens: does deamidation contribute to crystallin insolubility? Journal of Proteome Research 2006, 5, 2554–2566. [PubMed: 17022627]

Author Manuscript Author Manuscript Author Manuscript Author Manuscript

(18). Lampi KJ; Wilmarth PA; Murray MR; David LL Lens β-crystallins: the role of deamidation and related modifications in aging and cataract. Progress in Biophysics and Molecular Biology 2014, 115, 21–31. [PubMed: 24613629]

(19). Harrington V; McCall S; Huynh S; Srivastava K; Srivastava OP Crystallins in water soluble-high molecular weight protein fractions and water insoluble protein fractions in aging and cataractous human lenses. Mol Vis 2004, 10, 476–489. [PubMed: 15303090]

(20). Lampi KJ; Ma Z; Hanson SR; Azuma M; Shih M; Shearer TR; Smith DL; Smith JB; David LL Age-related changes in human lens crystallins identified by two-dimensional electrophoresis and mass spectrometry. Experimental Eye Research 1998, 67, 31–43. [PubMed: 9702176]

(21). Forsythe HM; Vetter CJ; Jara KA; Reardon PN; David LL; Barbar EJ; Lampi KJ Altered protein dynamics and increased aggregation of human γS-crystallin due to cataract-associated deamidations. Biochemistry 2019, 58, 4112–4124. [PubMed: 31490062]

(22). Vetter CJ; Thorn DC; Wheeler SG; Mundorff C; Halverson K; Carver JA; David LL; Lampi KJ Accumulative deamidation of human lens protein γS-crystallin leads to partially unfolded intermediates with enhanced aggregation propensity. bioRxiv 2020, doi: 10.1101/2020.02.21.960237.

(23). Fujii N; Momose Y; Ishibashi Y; Uemura T; Takita M; Takehana M Specific racemization and isomerization of the aspartyl residue of αA-crystallin due to UV-B irradiation. Experimental Eye Research 1997, 65, 99–104. [PubMed: 9237870]

(24). Hooi MYS; Raftery MJ; Truscott RJW Racemization of two proteins over our lifespan: deamidation of asparagine 76 in γS crystallin is greater in cataract than in normal lenses across the age range. Investigative Ophthalmology and Visual Science 2012, 53, 3554–3561. [PubMed: 22531704]

(25). Hains PG; Truscott RJ Proteomic analysis of the oxidation of cysteine residues in human age-related nuclear cataract lenses. Biochimica et Biophysica Acta (BBA)-Proteins and Proteomics 2008, 1784, 1959–1964. [PubMed: 18761110]

(26). Linetsky M; Ortwerth B Quantitation of the singlet oxygen produced by UVA irradiation of human lens proteins. Photochemistry and Photobiology 1997, 65, 522–529. [PubMed: 9077138]

(27). Zigman S Environmental near-UV radiation and cataracts. Optometry and Vision Science 1995, 72, 899–901. [PubMed: 8749337]

(28). Ghosh KS; Pande A; Pande J Binding of γ-crystallin substrate prevents the binding of copper and zinc ions to the molecular chaperone α-crystallin. Biochemistry 2011, 50, 3279–3281. [PubMed: 21417258]

(29). Cekic O Effect of cigarette smoking on copper, lead, and cadmium accumulation in human lens. British Journal of Ophthalmology 1998, 82, 186–188.

(30). Balaji M; Sasikala K; Ravindran T Copper levels in human mixed, nuclear brunescence, and posterior subcapsular cataract. British Journal of Ophthalmology 1992, 76, 668–669.

(31). Rácz P; Ördögh M Investigations on trace elements in normal and senile cataractous lenses. Albrecht von Graefes Archiv für Klinische und Experimentelle Ophthalmologie 1977, 204, 67–72. [PubMed: 303483]

(32). Aydin E; Cumurcu T; Özuĝurlu F; Özyurt H; Sahinoglu S; Mendil D; Hasdemir E Levels of iron, zinc, and copper in aqueous humor, lens, and serum in nondiabetic and diabetic patients. Biological Trace Element Research 2005, 108, 33–41. [PubMed: 16327057]

(33). Ahmad A; Ahmad I; Khan MA; Munshi AB; Siddiqui I; Anzar O; Anzar A On-Set of Cataract and Accumulation of Copper, Lead and Cadmium in Smokers of Karachi, Pakistan. Journal of Environmental & Analytical Toxicology 2015, 5, 1.

(34). Langford-Smith A; Tilakaratna V; Lythgoe PR; Clark SJ; Bishop PN; Day AJ Age and smoking related changes in metal ion levels in human lens: implications for cataract formation. PloS One 2016, 11, e0147576. [PubMed: 26794210]

(35). Roskamp KW; Kozlyuk N; Sengupta S; Bierma JC; Martin RW Divalent cations and the divergence of βγ-crystallin function. Biochemistry 2019, 58, 4505–4518. [PubMed: 31647219]

(36). Tabner BJ; Turnbull S; El-Aganf O; Allsop D Production of reactive oxygen species from aggregating proteins implicated in Alzheimer's disease, Parkinson's disease and other

Author Manuscript Author Manuscript Author Manuscript Author Manuscript

neurodegenerative diseases. Current Topics in Medicinal Chemistry 2001, 1, 507–517. [PubMed: 11895127]

(37). Manoharan S; Guillemin GJ; Abiramasundari RS; Essa MM; Akbar M; Akbar MD The role of reactive oxygen species in the pathogenesis of Alzheimer's disease, Parkinson's disease, and Huntington's disease: a mini review. Oxidative Medicine and Cellular Longevity 2016, 2016: 8590578. [PubMed: 28116038]

(38). Binolfi A; Quintanar L; Bertoncini CW; Griesinger C; Fernández CO Bioinorganic chemistry of copper coordination to alpha-synuclein: Relevance to Parkinson's disease. Coordination Chemistry Reviews 2012, 256, 2188–2201.

(39). Wang X; Moualla D; Wright JA; Brown DR Copper binding regulates intracellular alpha-synuclein localisation, aggregation and toxicity. Journal of Neurochemistry 2010, 113, 704–714. [PubMed: 20141569]

(40). Bush AI The metallobiology of Alzheimer's disease. Trends in Neurosciences 2003, 26, 207–214. [PubMed: 12689772]

(41). Faller P; Hureau C; La Penna G Metal ions and intrinsically disordered proteins and peptides: from Cu/Zn amyloid-β to general principles. Accounts of Chemical Research 2014, 47, 2252–2259. [PubMed: 24871565]

(42). Arnesano F; Scintilla S; Calò V; Bonfrate E; Ingrosso C; Losacco M; Pellegrino T; Rizzarelli E; Natile G Copper-triggered aggregation of ubiquitin. PloS One 2009, 4, e7052. [PubMed: 19756145]

(43). Bocharova OV; Breydo L; Salnikov VV; Baskakov IV Copper (II) inhibits in vitro conversion of prion protein into amyloid fibrils. Biochemistry 2005, 44, 6776–6787. [PubMed: 15865423]

(44). Zhou L-X; Du J-T; Zeng Z-Y; Wu W-H; Zhao Y-F; Kanazawa K; Ishizuka Y; Nemoto T; Nakanishi H; Li Y-M Copper (II) modulates in vitro aggregation of a tau peptide. Peptides 2007, 28, 2229–2234. [PubMed: 17919778]

(45). Wang X; Garcia CM; Shui Y-B; Beebe DC Expression and regulation of α-, β-, and γ-crystallins in mammalian lens epithelial cells. Investigative Ophthalmology and Visual Science 2004, 45, 3608–3619. [PubMed: 15452068]

(46). Robinson NE; Lampi KJ; Speir JP; Kruppa G; Easterling M; Robinson AB Quantitative measurement of young human eye lens crystallins by direct injection Fourier transform ion cyclotron resonance mass spectrometry. Molecular Vision 2006, 12, 704–711. [PubMed: 16807530]

(47). Siezen RJ; Thomson JA; Kaplan ED; Benedek GB Human lens gamma-crystallins: isolation, identification, and characterization of the expressed gene products. Proceedings of the National Academy of Sciences 1987, 84, 6088–6092.

(48). Konz I; B. F; Fernández M; Pereiro R; González-Iglesias H; Coca-Prados M; Sanz-Medel A Quantitative bioimaging of trace elements in the human lens by LAICP-MS. Analytical and Bioanalytical Chemistry 2014, 406, 2343–2348. [PubMed: 24500754]

(49). Quintanar L; Domínguez-Calva J; Serebryany E; Rivillas-Acevedo L; Haase-Pettingell C; Amero C; King J Copper and zinc ions specifically promote nonamyloid aggregation of the highly stable human γ-D crystallin. ACS Chemical Biology 2015, 11, 263–272. [PubMed: 26579725]

(50). Bloemendal H; de Jong W; Jaenicke R; Lubsen NH; Slingsby C; Tardieu A Ageing and vision: structure, stability and function of lens crystallins. Progress in Biophysics and Molecular Biology 2004, 86, 407–485. [PubMed: 15302206]

(51). Serebryany E; Yu S; Trauger SA; Budnik B; Shakhnovich EI Dynamic disulfide exchange in a crystallin protein in the human eye lens promotes cataract-associated aggregation. Journal of Biological Chemistry 2018, 293, 17997–18009.

(52). Sweeney MH; Truscott RJ An impediment to glutathione diffusion in older normal human lenses: A possible precondition for nuclear cataract. Experimental Eye Research 1998, 67, 587–595. [PubMed: 9878221]

(53). Studier FW Protein production by auto-induction in high-density shaking cultures. Protein Expression and Purification 2005, 41, 207–234. [PubMed: 15915565]

Author Manuscript Author Manuscript Author Manuscript Author Manuscript

(54). Roskamp KW; Montelongo DM; Anorma CD; Bandak DN; Chua JA; Malecha KT; Martin RW Multiple aggregation pathways in human γS-xrystallin and Its aggregation-prone G18V variant. Investigative Ophthalmology and Visual Science 2017, 58, 2397–2405. [PubMed: 28444328]

(55). Khago D; Wong EK; Kingsley CN; Freites JA; Tobias DJ; Martin RW Increased hydrophobic surface exposure in the cataract-related G18V variant of human γS-crystallin. Biochimica et Biophysica Acta (BBA)-General Subjects 2016, 1860, 325–332. [PubMed: 26459004]

(56). R Core Team, R: A Language and Environment for Statistical Computing. R Foundation for Statistical Computing: Vienna, Austria, 2015.

(57). Liu Y Package 'Ritc': Isothermal Titration Calorimetry (ITC) Data Analysis. Johns Hopkins University: Baltimore, Maryland, 2016.

(58). Eftink M; Selvidge L Fluorescence quenching of liver alcohol dehydrogenase by acrylamide. Biochemistry 1982, 21, 117–125. [PubMed: 7037051]

(59). Gordon SE; Senning EN; Aman TK; Zagotta WN Transition metal ion FRET to measure short-range distances at the intracellular surface of the plasma membrane. The Journal of General Physiology 2016, 147, 189–200. [PubMed: 26755772]

(60). Pande A; Annunziata O; Asherie N; Ogun O; Benedek GB; Pande J Decrease in protein solubility and cataract formation caused by the Pro23 to Thr mutation in human γD-crystallin. Biochemistry 2005, 44, 2491–2500. [PubMed: 15709761]

(61). Boatz JC; Whitley MJ; Li M; Gronenborn AM; van der Wel PC Cataract-associated P23T γD-crystallin retains a native-like fold in amorphous-looking aggregates formed at physiological pH. Nature Communications 2017, 8, 15137.

(62). Karri S; Kasetti RB; Vendra VPR; Chandani S; Balasubramanian D Structural analysis of the mutant protein D26G of human γS-crystallin, associated with Coppock cataract. Molecular Vision 2013, 19, 1231–1237. [PubMed: 23761725]

(63). Bharat SV; Shekhtman A; Pande J The cataract-associated V41M mutant of human γS-crystallin shows specific structural changes that directly enhance local surface hydrophobicity. Biochemical and Biophysical Research Communications 2014, 443, 110–114. [PubMed: 24287181]

(64). Brubaker WD; Martin RW 1 H, 13 C, and 15 N assignments of wild-type human γS-crystallin and its cataract-related variant γS-G18V. Biomolecular NMR Assignments 2012, 6, 63–67. [PubMed: 21735120]

(65). Haris PI; Severcan F FTIR spectroscopic characterization of protein structure in aqueous and non-aqueous media. Journal of Molecular Catalysis B: Enzymatic 1999, 7, 207–221.

(66). Fatima U; Sharma S; Guptasarma P Structures of differently aggregated and precipitated forms of γB crystallin: An FTIR spectroscopic and EM study. Protein and Peptide Letters 2010, 17, 1155–1162. [PubMed: 20394579]

(67). Vendra VPR; Chandani S; Balasubramanian D The mutation V42M distorts the compact packing of the human gamma-S-crystallin molecule, resulting in congenital cataract. PLoS One 2012, 7, e51401. [PubMed: 23284690]

(68). Ji F; Jung J; Koharudin LM; Gronenborn AM The human W42R γD-crystallin mutant structure provides a link between congenital and age-related cataracts. Journal of Biological Chemistry 2013, 288, 99–109.

(69). Talla V; Narayanan C; Srinivasan N; Balasubramanian D Mutation causing self-aggregation in human γC-crystallin leading to congenital cataract. Investigative Ophthalmology & Visual Science 2006, 47, 5212–5217. [PubMed: 17122105]

(70). Matulis D; Baumann CG; Bloomfield VA; Lovrien RE 1-Anilino-8-naphthalene sulfonate as a protein conformational tightening agent. Biopolymers: Original Research on Biomolecules 1999, 49, 451–458.

(71). Kim I; Saito T; Fujii N; Kanamoto T; Chatake T; Fujii N Site specific oxidation of amino acid residues in rat lens γ-crystallin induced by low-dose γ-irradiation. Biochemical and Biophysical Research Communications 2015, 466, 622–628. [PubMed: 26385181]

(72). Ramkumar S; Fan X; Wang B; Yang S; Monnier VM Reactive cysteine residues in the oxidative dimerization and Cu2+ induced aggregation of human γD-crystallin: Implications for age-related cataract. Biochimica et Biophysica Acta (BBA)-Molecular Basis of Disease 2018, 1864, 3595–3604. [PubMed: 30251679]

Author Manuscript Author Manuscript Author Manuscript Author Manuscript

(73). Domínguez-Calva JA; Haase-Pettingell C; Serebryany E; King JA; Quintanar L A Histidine Switch for Zn-Induced Aggregation of γ-Crystallins Reveals a Metal-Bridging Mechanism That Is Relevant to Cataract Disease. Biochemistry 2018, 57, 4959–4962. [PubMed: 30064223]

(74). Domínguez-Calva J; Pérez-Vázquez M; Serebryany E; King J; Quintanar L Mercury-induced aggregation of human lens γ-crystallins reveals a potential role in cataract disease. JBIC Journal of Biological Inorganic Chemistry 2018, 23, 1–14. [PubMed: 29218638]

(75). Smith R; Martell A; Motekaitis R NIST standard reference database 46. NIST, 2004.

(76). Xiao Z; Brose J; Schimo S; Ackland SM; La Fontaine S; Wedd AG Unification of the copper (I) binding affinities of the metallo-chaperones Atx1, Atox1, and related proteins detection probes and affinity standards. Journal of Biological Chemistry 2011, 286, 11047–11055.

(77). Krżel A; Leśniak W; Jeżowska-Bojczuk M; Młynarz P; Brasuñ J; Kozłowski H; Bal W Coordination of heavy metals by dithiothreitol, a commonly used thiol group protectant. Journal of Inorganic Biochemistry 2001, 84, 77–88. [PubMed: 11330484]

(78). Flaugh SL; Kosinski-Collins MS; King J Contributions of hydrophobic domain interface interactions to the folding and stability of human γD-crystallin. Protein Science 2005, 14, 569–581. [PubMed: 15722442]

(79). Kosinski-Collins MS; Flaugh SL; King J Probing folding and fluorescence quenching in human γD crystallin Greek key domains using triple tryptophan mutant proteins. Protein Science 2004, 13, 2223–2235. [PubMed: 15273315]

(80). Ma Z; Piszczek G; Wingfield PT; Sergeev YV; Hejtmancik JF The G18V CRYGS mutation associated with human cataracts increases γS-crystallin sensitivity to thermal and chemical stress. Biochemistry 2009, 48, 7334–7341. [PubMed: 19558189]

(81). Moreau KL; King J Hydrophobic core mutations associated with cataract development in mice destabilize human γD-crystallin. Journal of Biological Chemistry 2009, 284, 33285–33295.

(82). Whitley MJ; Xi Z; Bartko JC; Jensen MR; Blackledge M; Gronenborn AM A combined NMR and SAXS analysis of the partially folded cataract-associated V75D γD-crystallin. Biophysical Journal 2017, 112, 1135–1146. [PubMed: 28355541]

(83). Changela A; Chen K; Xue Y; Holschen J; Outten CE; O'Halloran TV; Mondragón A Molecular basis of metal-ion selectivity and zeptomolar sensitivity by CueR. Science 2003, 301, 1383–1387. [PubMed: 12958362]

(84). Lu C-H; Lin Y-F; Lin J-J; Yu C-S Prediction of metal ion–binding sites in proteins using the fragment transformation method. PloS One 2012, 7, e39252. [PubMed: 22723976]

(85). Lin Y-F; Cheng C-W; Shih C-S; Hwang J-K; Yu C-S; Lu C-H MIB: metal ion-binding site prediction and docking server. Journal of Chemical Information and Modeling 2016, 56, 2287–2291. [PubMed: 27976886]

(86). Brose J; La Fontaine S; Wedd AG; Xiao Z Redox sulfur chemistry of the copper chaperone Atox1 is regulated by the enzyme glutaredoxin 1, the reduction potential of the glutathione couple GSSG/2GSH and the availability of Cu (I). Metallomics 2014, 6, 793–808. [PubMed: 24522867]

(87). Zimmermann M; Clarke O; Gulbis JM; Keizer DW; Jarvis RS; Cobbett CS; Hinds MG; Xiao Z; Wedd AG Metal binding affinities of Arabidopsis zinc and copper transporters: selectivities match the relative, but not the absolute, affinities of their amino-terminal domains. Biochemistry 2009, 48, 11640–11654. [PubMed: 19883117]

(88). North ML; Wilcox DE Shift from Entropic Cu2+ Binding to Enthalpic Cu+ Binding Determines the Reduction Thermodynamics of Blue Copper Proteins. Journal of the American Chemical Society 2019, 141, 14329–14339. [PubMed: 31433629]

(89). Kanwar R; Balasubramanian D Structure and stability of the dityrosine-linked dimer of γB-crystallin. Experimental Eye Research 1999, 68, 773–784. [PubMed: 10375441]

(90). Buhr F; Jha S; Thommen M; Mittelstaet J; Kutz F; Schwalbe H; Rodnina MV; Komar AA Synonymous codons direct cotranslational folding toward different protein conformations. Molecular Cell 2016, 61, 341–351. [PubMed: 26849192]

(91). Thorn DC; Grosas AB; Mabbitt PD; Ray NJ; Jackson CJ; Carver JA The structure and stability of the disulfide-linked γS-crystallin dimer provide insight into oxidation products associated with lens cataract formation. Journal of molecular biology 2019, 431, 483–497. [PubMed: 30552875]

Author Manuscript Author Manuscript Author Manuscript Author Manuscript

(92). Abajian C; Yatsunyk LA; Ramirez BE; Rosenzweig AC Yeast Cox17 solution structure and copper (I) binding. Journal of Biological Chemistry 2004, 279, 53584–53592.

(93). Wernimont AK; Huffman DL; Lamb AL; O'Halloran TV; Rosenzweig AC Structural basis for copper transfer by the metallochaperone for the Menkes/Wilson disease proteins. Nature Structural & Molecular Biology 2000, 7, 766–771.

(94). Rosenzweig AC; O'Halloran TV Structure and chemistry of the copper chaperone proteins. Current Opinion in Chemical Biology 2000, 4, 140–147. [PubMed: 10742187]

(95). Banci L; Bertini I; Cantini F; Felli IC; Gonnelli L; Hadjiliadis N; Pierattelli R; Rosato A; Voulgaris P The Atx1-Ccc2 complex is a metal-mediated protein-protein interaction. Nature Chemical Biology 2006, 2, 367–368. [PubMed: 16732294]

(96). Fountoulakis M; Juranville J-F; Stüber D; Weibel EK; Garotta G Purification and biochemical characterization of a soluble human interferon gamma receptor expressed in Escherichia coli. Journal of Biological Chemistry 1990, 265, 13268–13275.

(97). Taniyama Y; Kuroki R; Omura F; Seko C; Kikuchi M Evidence for intramolecular disulfide bond shuffling in the folding of mutant human lysozyme. Journal of Biological Chemistry 1991, 266, 6456–6461.

(98). Chen W; Li L; Du Z; Liu J; Reitter JN; Mills KV; Linhardt RJ; Wang C Intramolecular disulfide bond between catalytic cysteines in an intein precursor. Journal of the American Chemical Society 2012, 134, 2500–2503. [PubMed: 22280304]

(99). Shelake RM; Ito Y; Masumoto J; Morita EH; Hayashi H A novel mechanism of 'metal gel-shift' by histidine-rich Ni^{2+}-binding Hpn protein from *Helicobacter pylori* strain SS1. PloS One 2017, 12, e0172182. [PubMed: 28207866]

(100). Khago D; Bierma JC; Roskamp KW; Kozlyuk N; Martin RW Protein refractive index increment is determined by conformation as well as composition. Journal of Physics: Condensed Matter 2018, 30, 435101. [PubMed: 30280702]

(101). Ma Z; Hanson SR; Lampi KJ; David LL; Smith DL; Smith JB Age-related changes in human lens crystallins identified by HPLC and mass spectrometry. Experimental Eye Research 1998, 67, 21–30. [PubMed: 9702175]

(102). Hanson SR; Smith DL; Smith JB Deamidation and disulfide bonding in human lens γ-crystallins. Experimental Eye Research 1998, 67, 301–312. [PubMed: 9778411]

(103). Skouri-Paneta F; Bonneté F; Prata K; Bateman OA; Lubsen HN; Tardieu A Lens crystallins and oxidation: the special case of γS. Biophysical Chemistry 2001, 89, 65–76. [PubMed: 11246746]

(104). Serebryany E;Woodard JC;Adkar BV;Shabab M;King JA; Shakhnovich EI An internal disulfide locks a misfolded aggregation-prone intermediate in cataract-linked mutants of human γD-crystallin. Journal of Biological Chemistry 2016, 291, 19172–19183.

(105). Kaiser CJ; Peters C; Schmid PW; Stavropoulou M; Zou J; Dahiya V; Mymrikov EV; Rockel B; Asami S; Haslbeck M; Rappsilber J; Reif B; Zacharias M; Buchner J; Weinkauf S The structure and oxidation of the eye lens chaperone αA-crystallin. Nature Structural & Molecular Biology 2019, 26, 1141–1150.

(106). Sagar V; Wistow G Mouse γS-crystallin L16 octamer. to be published 2018,

Author Manuscript Author Manuscript Author Manuscript Author Manuscript

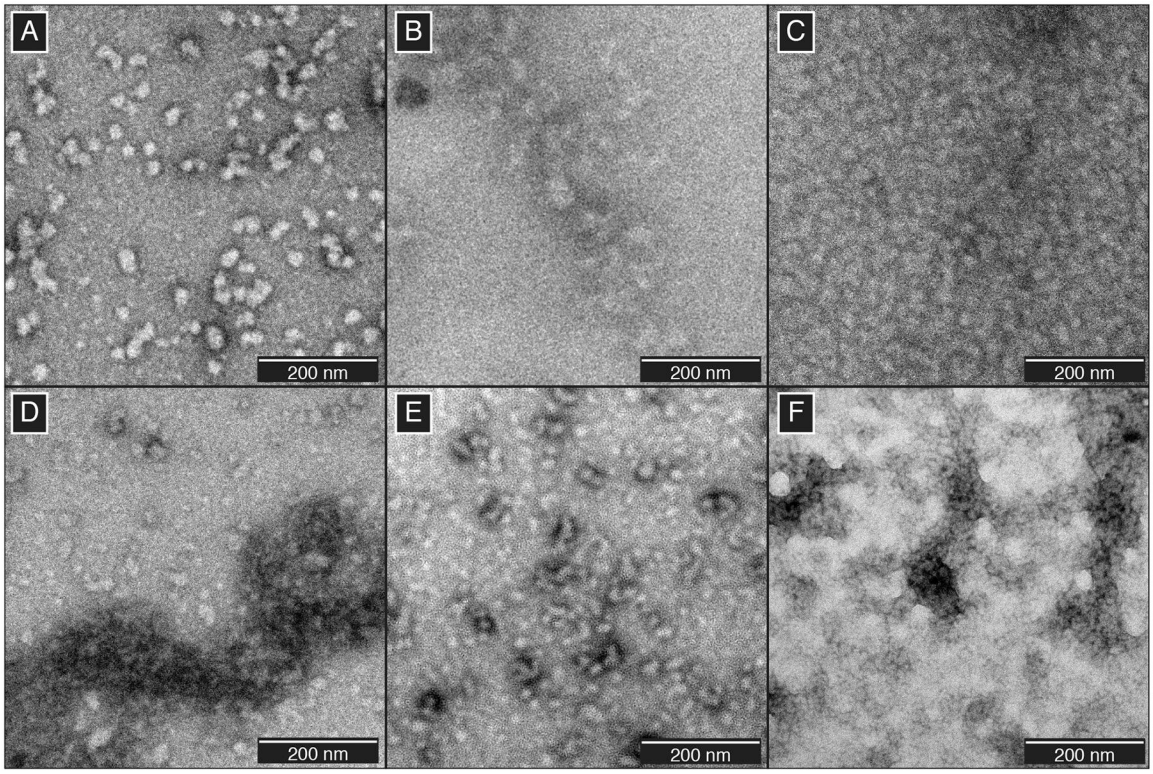

Figure 1:

TEM micrographs of γS-crystallin aggregates. (**A**) Native aggregates of γS-D26G, (**B**) γS-G18V, and (**C**) γS-V42M. Photodamaged aggregates formed using (**D**) UVA or (**E**) UVB radiation. (**F**) Aggregates resulting from the treatment of 0.5 equivalents of $CuCl_2$.

Author Manuscript Author Manuscript Author Manuscript Author Manuscript

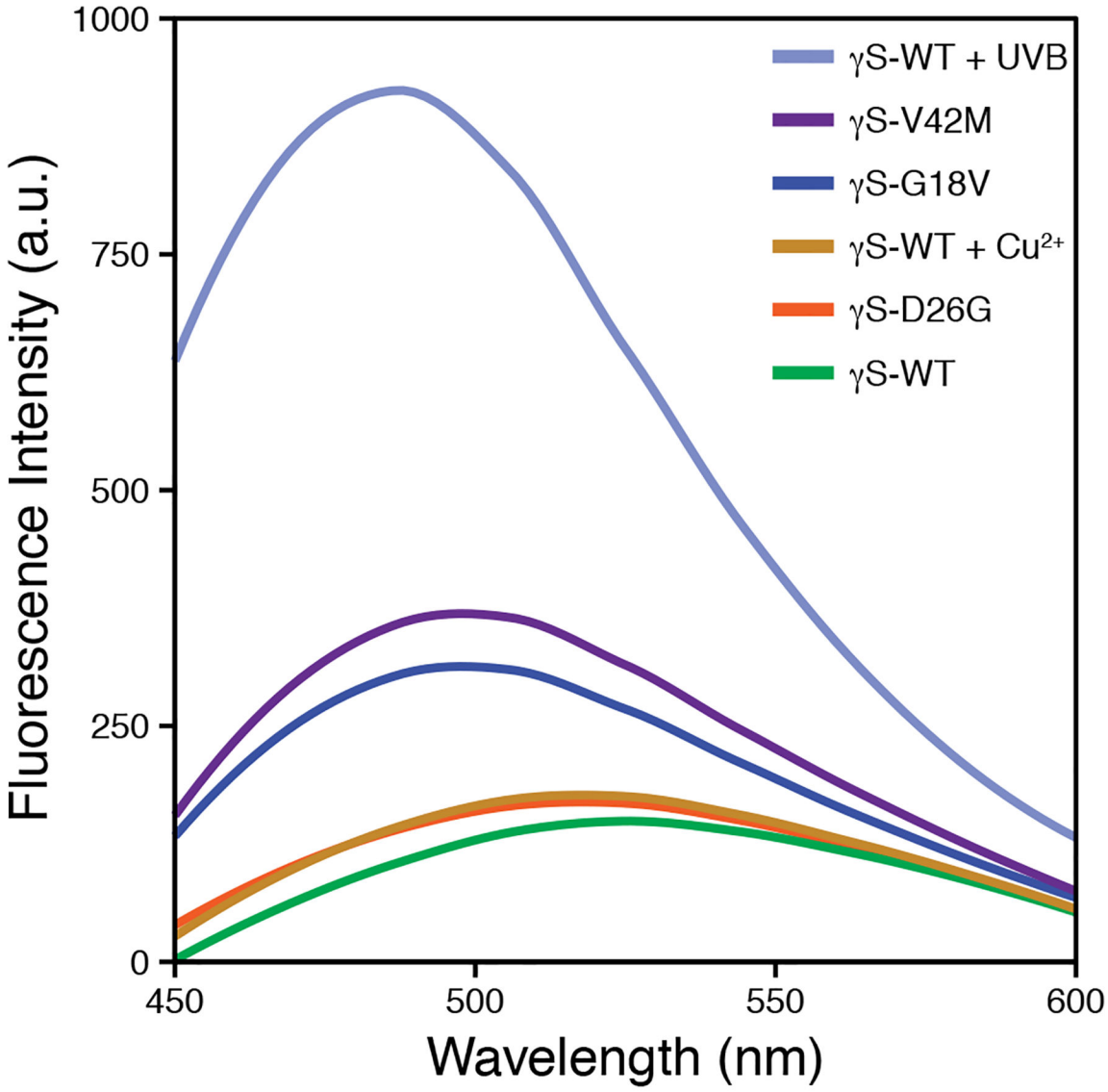

Figure 2:

Fluorescence spectra of ANS upon binding to γS-crystallins. In each case, 50 μM of soluble protein was incubated with 750 μM of ANS in order to probe changes in hydrophobic surface exposure. UVB irradiation produces considerable hydrophobic exposure. The soluble γS-WT remaining after $CuCl_2$ addition exhibits minimal changes in its ANS fluorescence spectrum relative to that of γS-WT. Point-variant ANS fluorescence differences are consistent with previous reports.

Author Manuscript Author Manuscript Author Manuscript Author Manuscript

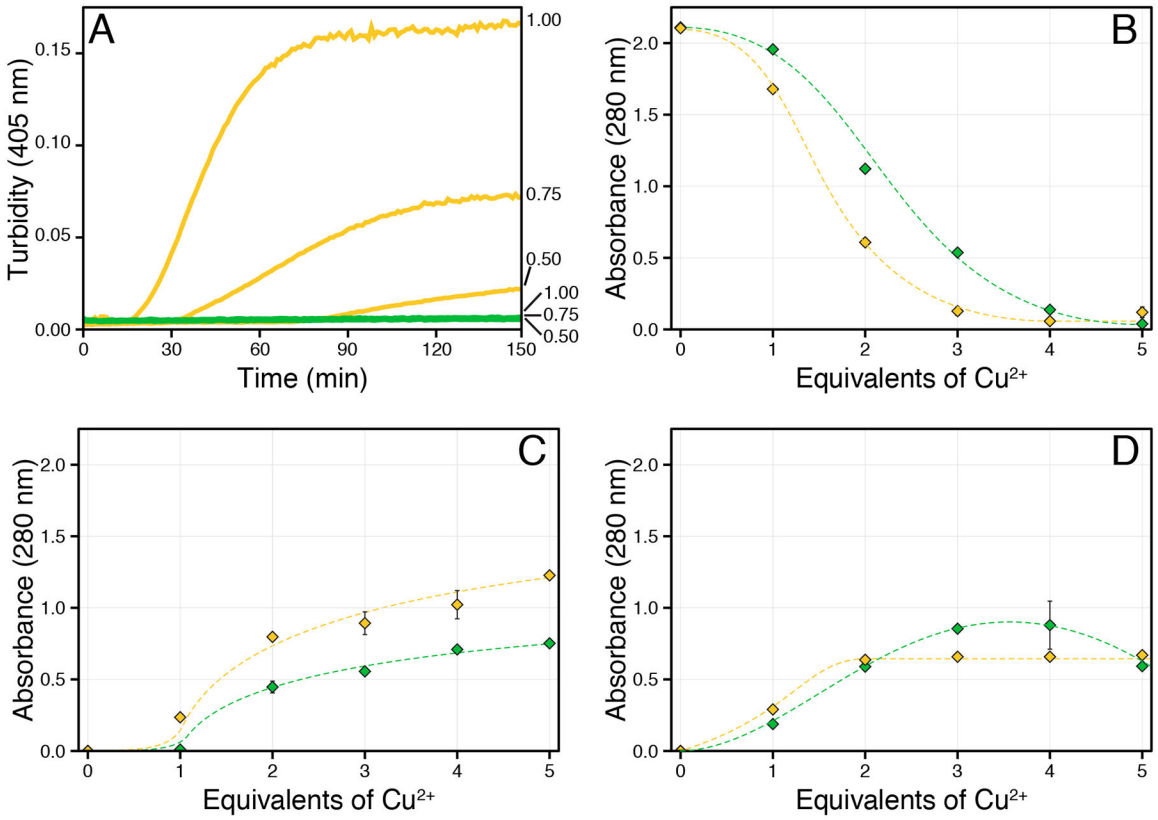

Figure 3:

The 280 nm absorbance of γS-WT (green) and γS-C_0 (gold) was measured following $CuCl_2$ addition. (**A**) Aggregation kinetics of γS-WT (green) and S-C_0 (gold) following the addition of 0.5, 0.75, or 1 equivalent of $CuCl_2$ (listed on right). After 150 minutes, no turbidity was observed for γS-WT, whereas the onset and extent of γS-C_0 turbidity increased with copper concentration. (**B**) Absorbance of the supernatant following centrifugation. (**C**) The absorbance of proteins resuspended from copper-induced aggregation via EDTA. (**D**) The absorbance of proteins resuspended from copper-induced aggregation via DTT. Error bars represent one standard deviation. The lines serve as a visual guide.

Author Manuscript Author Manuscript Author Manuscript Author Manuscript

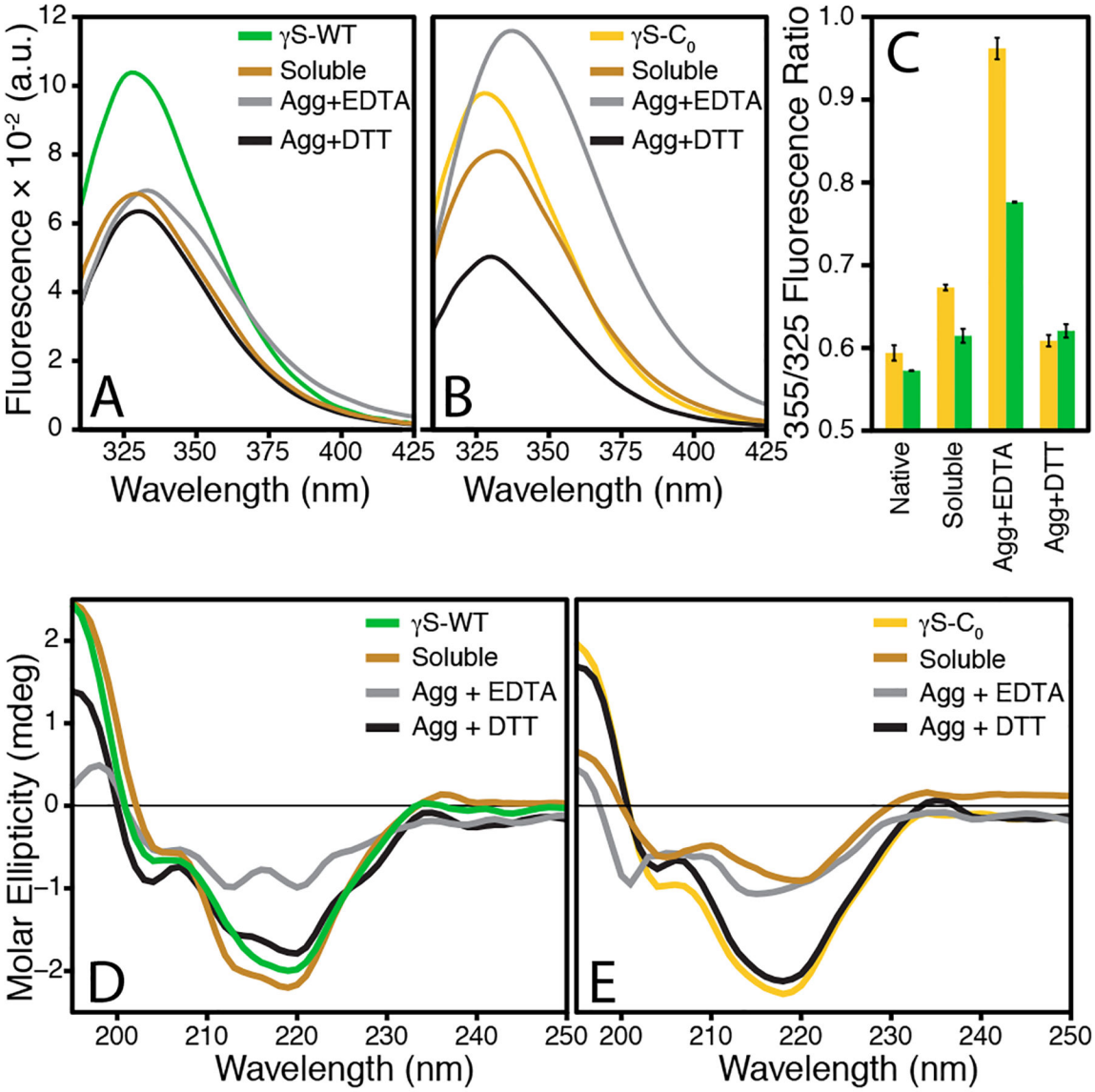

Figure 4:

Fluorescence and CD spectra of soluble and aggregated γS-WT and γS-C_0 after incubation with 2 equivalents of $CuCl_2$. Both EDTA-resolubilized species exhibit the greatest extent of unfolding, with considerably more unfolding occurring in γS-C_0 than γS-WT. (**A**) Fluorescence of untreated and copper-incubated samples of γS-WT. (**B**) Fluorescence of untreated and copper-incubated samples of γS-C_0. (**C**) The 355 nm over 325 nm fluorescence intensity ratio for each of the samples measured in parts (**A**) and (**B**). Error bars represent one standard deviation. (**D**) CD of untreated and copper-incubated samples of γS-WT. (**E**) CD of untreated and copper-incubated samples of γS-C_0.

Author Manuscript Author Manuscript Author Manuscript Author Manuscript

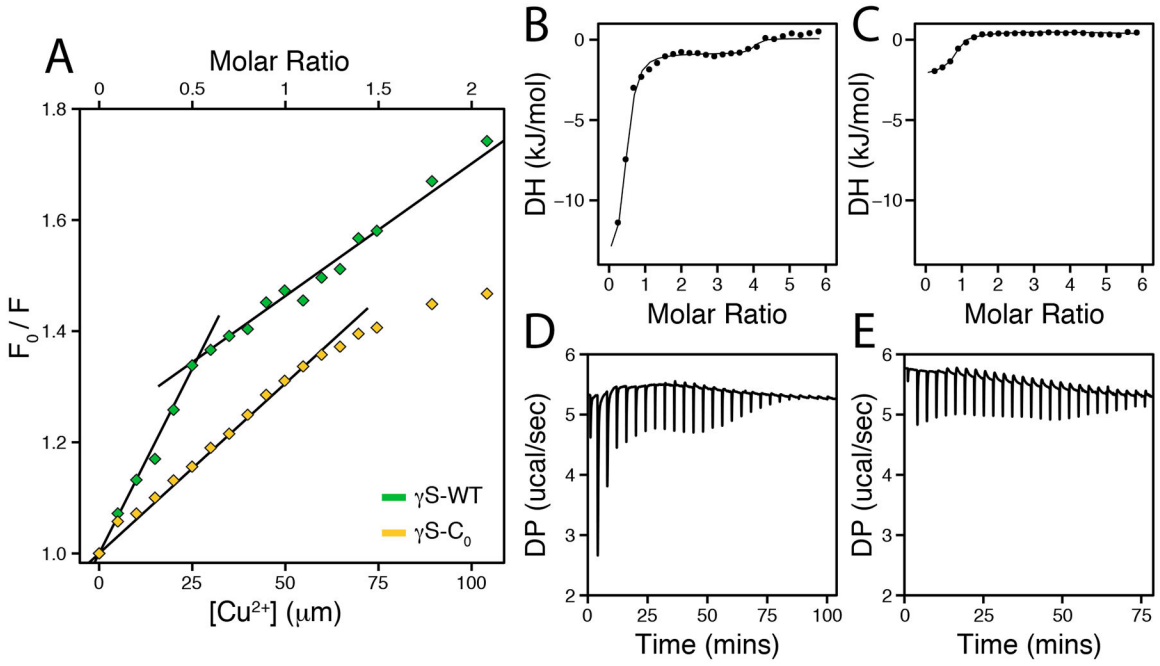

Figure 5:

(**A**) Stern-Volmer plots of the fluorescence quenching for γS-WT (green) and γS-C_0 (gold) resulting from $CuCl_2$ titration. The plotted data show the ratio of the initial fluorescence intensity at 330 nm to the intensity following $CuCl_2$ addition. The S-WT data after 0.5 equivalents were fit to a second model. Data up to 1.5 equivalents were used for for γS-C_0. (**B-C**) Integrated heat and (**D-E**) raw data from isothermal titration calorimetry measurements of γS-WT (**B, D**) and γS-C_0 (**C, E**) titrations with $CuCl_2$ at 25 °C.

Author Manuscript Author Manuscript Author Manuscript Author Manuscript

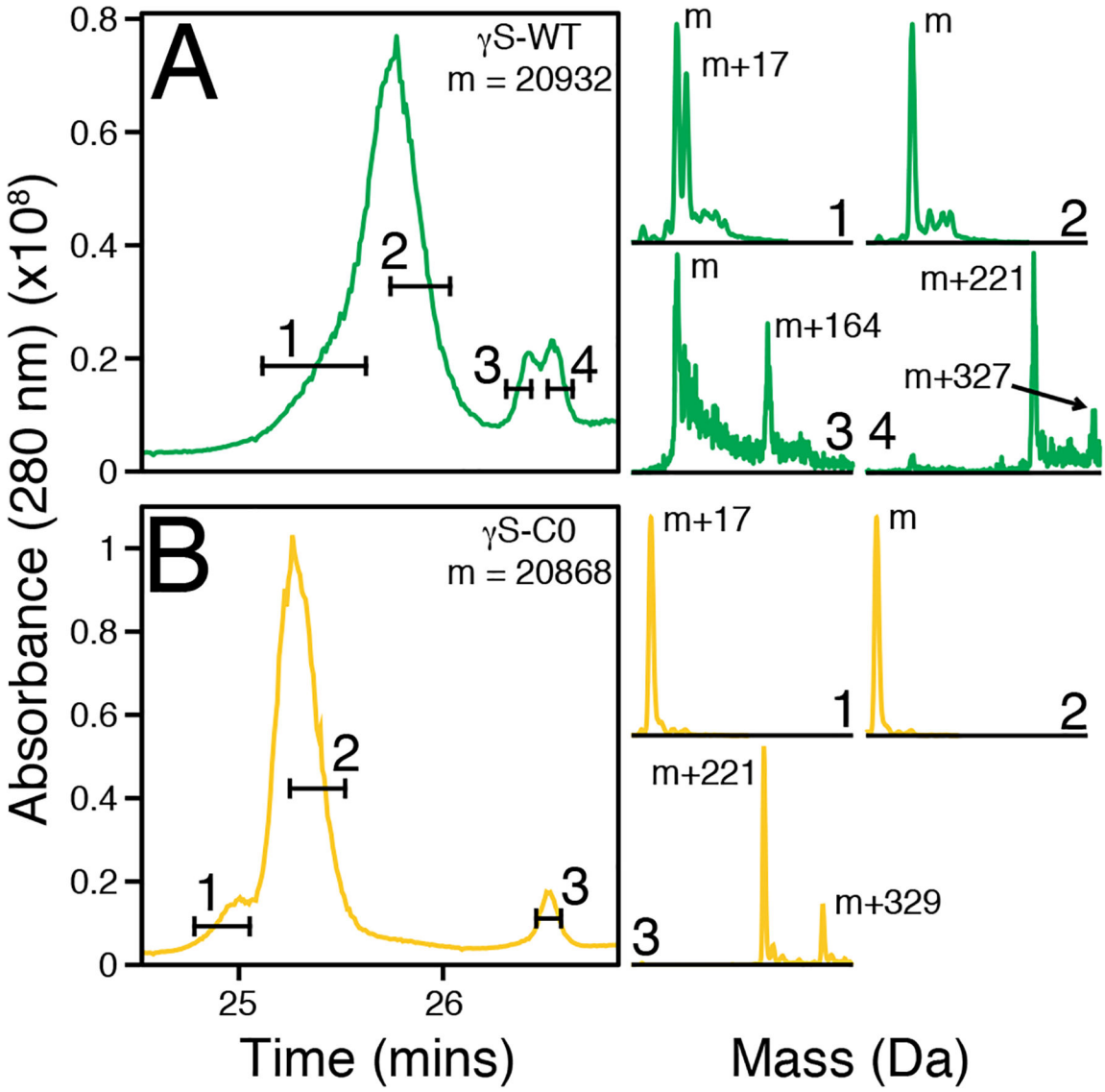

Figure 6:

The dimer peaks from chromatographic separation (analytical SEC) of γS-WT (**A**) and γS-C_0 (**B**) after EDTA resolubilization were separated on a C4 column prior to mass spectrometry. Two distinct peaks are visible for both proteins, with shouldering or splitting present for most peaks. The selected time frames drawn across the chromatographic traces correspond to the data used for the corresponding mass reconstructions. The fourth selected time frame for γS-WT and third selected time frame of γS-C_0 correspond to the same chromatographic retention time.

Author Manuscript Author Manuscript Author Manuscript Author Manuscript

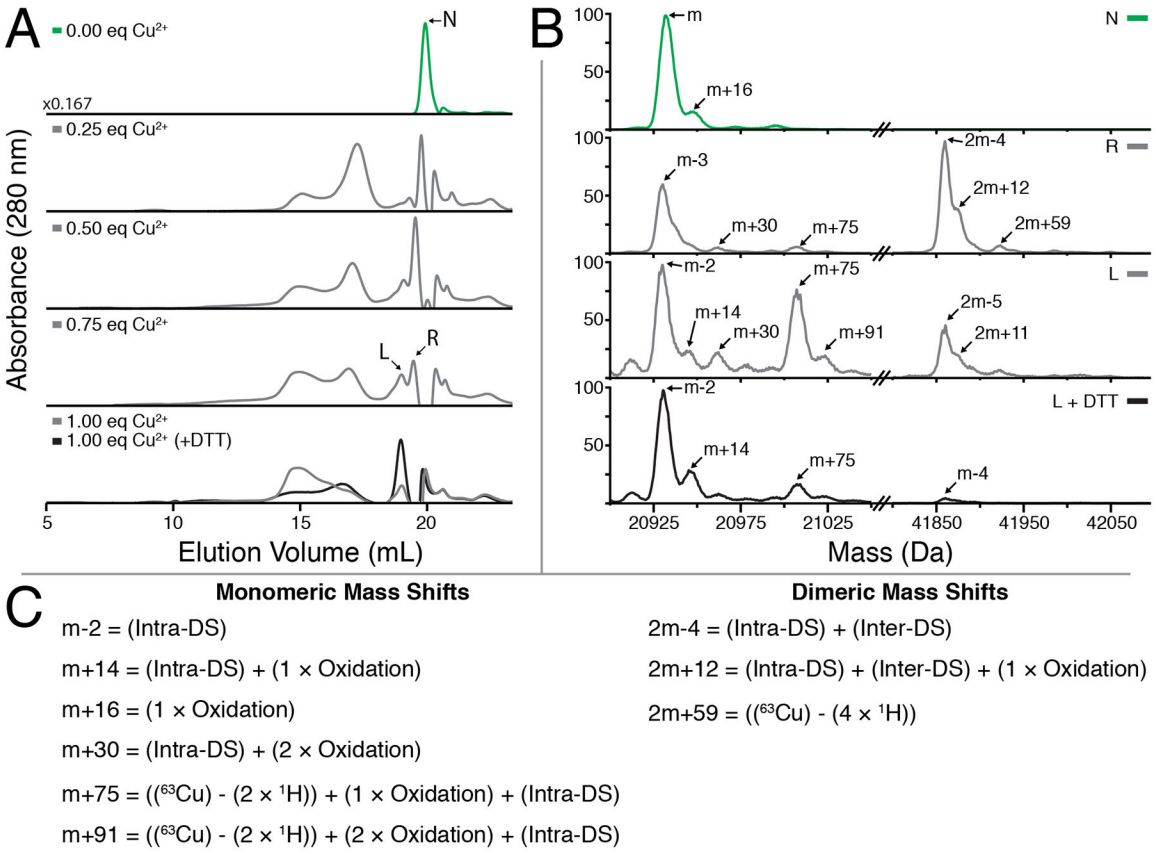

Figure 7:

(**A**) Analytical SEC measurements of γS-WT treated with increasing equivalents of $CuCl_2$ followed by excess EDTA. The addition of $CuCl_2$ results in dimerization of γS-WT, with a shift towards high molecular weight species with increasing concentration. Formation of these larger species is partly reversible upon DTT reduction. (bottom panel). (**B**) Protein masses reconstructed using MaxEnt1 for individual peaks collected in (**A**). The untreated γS-WT (U) is strictly monomeric, whereas the fractions eluting at the same time (R) and just before (L) following Copper treatment exhibit dimer character. Reduction via DTT considerably increases the total monomeric content of the L peak. (**C**) Modifications accounting for the observed mass shifts observed in part (**B**).

Author Manuscript Author Manuscript Author Manuscript Author Manuscript

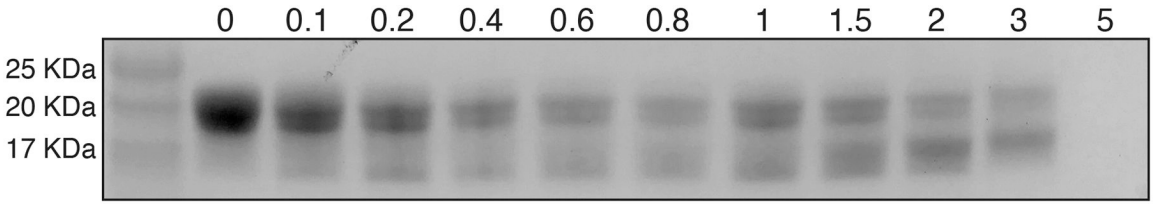

Figure 8:

SDS-PAGE analysis of γS-crystallin treated with variable amounts of $CuCl_2$. Soluble γS-WT after incubation with 0, 0.1, 0.2, 0.4, 0.6, 0.8, 1, 1.5, 2, 3, and 5 equiv of $CuCl_2$. Two bands are observed near ~20kDa beginning at 0.1 equiv of $CuCl_2$. A lower band below the 17 kDa protein standard is also clearly present after the addition of 0.2 equiv of $CuCl_2$. The lower gel band similarly splits into two close bands with increasing $CuCl_2$ concentrations. The small additional migration within each band pair corresponds to the formation of an intramolecular disulfide bond. The larger additionally migration causing the splitting of the band pairs is due to copper binding.

Author Manuscript Author Manuscript Author Manuscript Author Manuscript

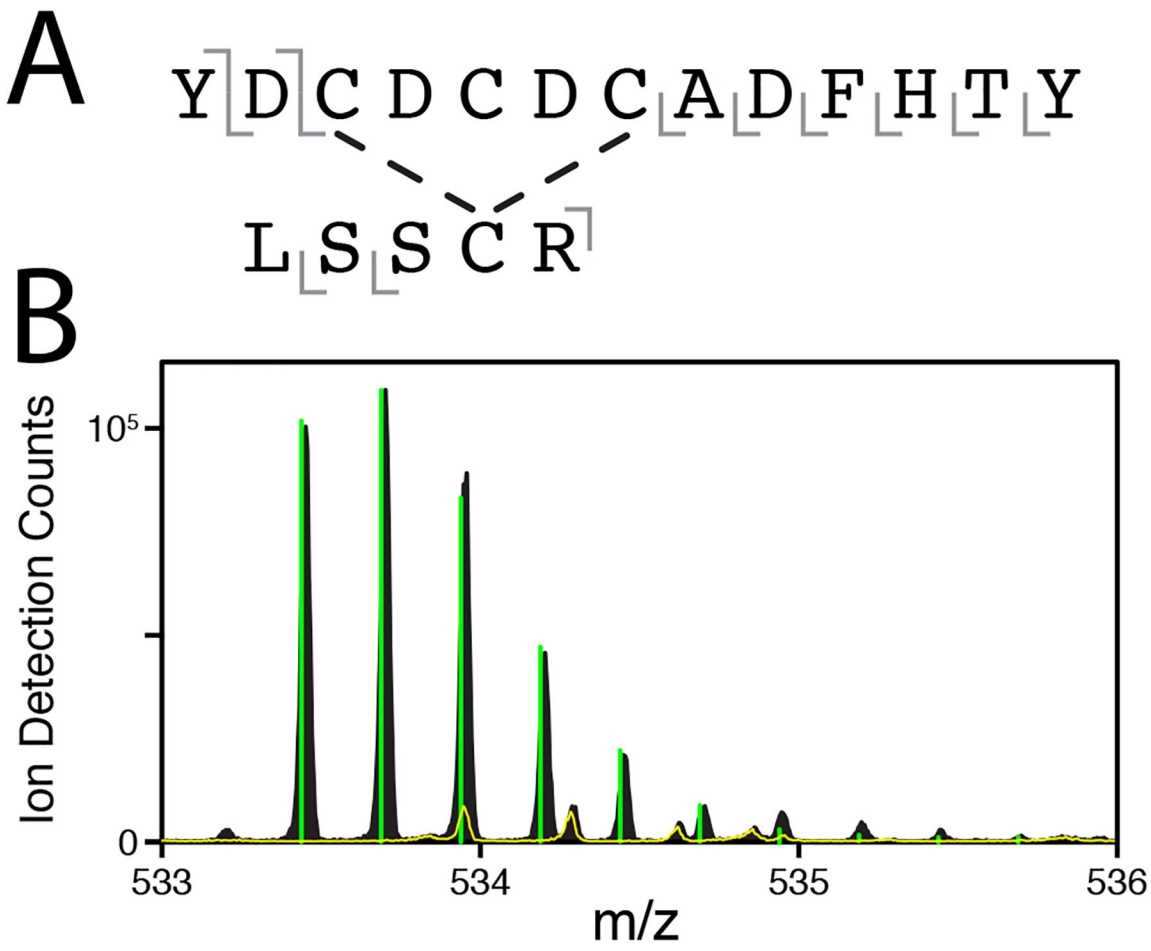

Figure 9:

(**A**) Primary structure of one peptide fragment containing an intramolecular disulfide bond. Gray bars indicate the location of fragmentation observed via MS/MS (detailed in SI Figures S11–S12 and SI Table S1).The location of the disulfide is not definitively assignable, but is most likely between C83 and either C23 or C27 based on the protein structure. (**B**) The mass to charge ratio peaks of the parent fragment with (yellow line) or without (black) DTT. Green bars represent the predicted isotope pattern of the parent fragment. The elimination of the parent peaks confirms a disulfide linkage.

Author Manuscript Author Manuscript Author Manuscript Author Manuscript

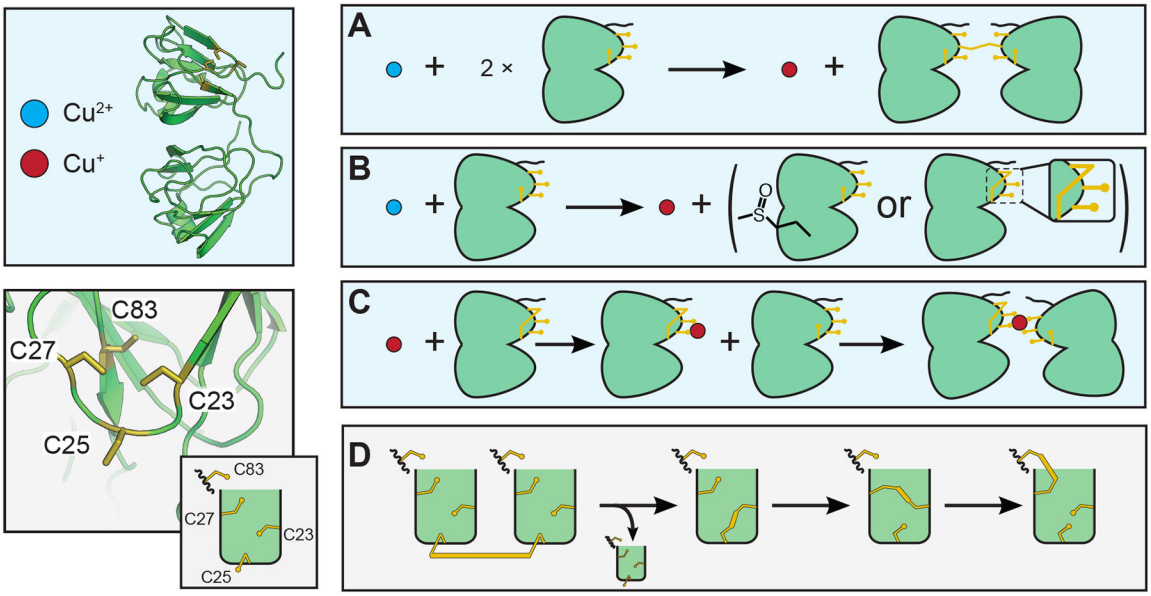

Figure 10:

Potential interactions of γS-crystallin involving copper and disulfide bond (shown in gold) transfers. (**A**) Reduction of Cu(II) to Cu(I) and oxidation of two γS-crystallins resulting in an intermolecular disulfide. (**B**) Cu(II) is reduced to Cu(I) while γS is oxidized. Oxidation may cause methionine sulfoxide, cysteine sulfenic acid, or intramolecular disulfide bond formation. (**C**) Cu(I) binding to γS-crystallin may lead to the formation of a metal-bridged dimer. (**D**) Disulfide bond transfer between γS-crystallins most likely involves C25. Although the exact transfer pathway is not yet known, it is clear that C83 is involved in the final intramolecular disulfide. So far the partner cysteine has not been definitively identified; however, barring a large structural rearrangement, C23 and/or C27 must be involved in any intermediary isomerization.

Author Manuscript Author Manuscript Author Manuscript Author Manuscript

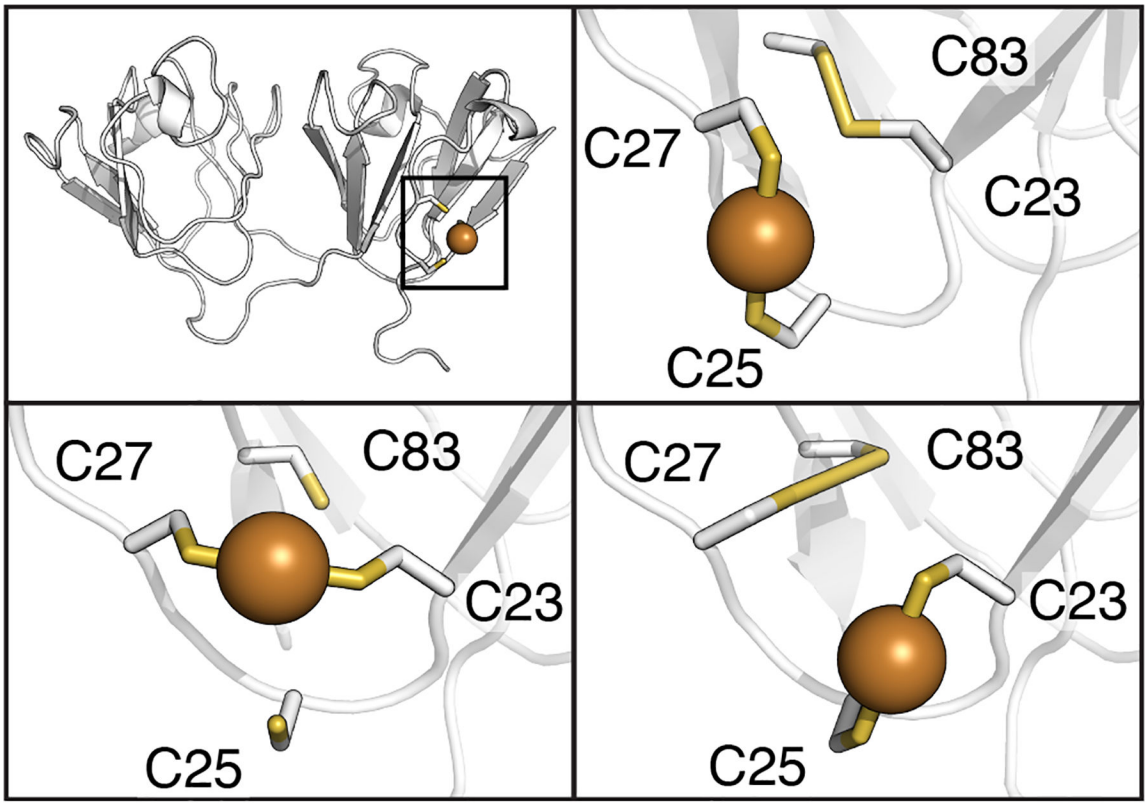

Figure 11:

Potential intramolecular disulfide bond and copper binding site interactions for γS-crystallin. The copper binding sites shown here involve ligands 180° apart with bond distances less than 2.4 Å. **(Top left)** The bonding interactions are localized to the cysteine loop area of the NTD. **(Top right)** Potential C23-C83 intramolecular disulfide bond and C25/C27 copper binding site modeled in γS-crystallin using PDBID 6MYG.[106] **(Bottom right)** Alternative possible intramolecular disulfide between C27-C83 and copper binding sites in γS-crystallin modeled using PDBID 2M3T.[64] **(Bottom left)** Copper binding site in S-crystallin between C23 and C27 modeled using PDBID 2M3T.[64]

Author Manuscript

Author Manuscript

Author Manuscript

Author Manuscript

Table 1:

Stern-Volmer binding constants determined via tmFRET for γS-crystallins and $CuCl_2$ at pH 7 and 25 °C. Rows 1 and 2 are different isotherms from the same sample of γS-WT.

Protein	$K_{SV\,1}$	$K_{SV\,2}$
γS-WT	12.1 (± 1.4) × 10^3	4.51 (± 0.4) × 10^3
γS-C_0	6.11 (± 0.3) × 10^3	

Author Manuscript

Author Manuscript

Author Manuscript

Author Manuscript

Table 2:

Average thermodynamic parameters for γS-crystallins and $CuCl_2$ at pH 7.0 and 25 °C.

Protein	n	K_{ITC} (M^{-1})	ΔH (kJ/mol)	ΔG (kJ/mol)	−TΔS (kJ/mol)
γS-WT	0.38 ± 0.01	4.7 (± 3.8) × 10^8	−55.6 ± 6.4	−42.6 ± 1.8	12.9 ± 7.5
γS-WT	3.70 ± 0.20	4.0 (± 4.0) × 10^6	−5.1 ± 1.0	−31.8 ± 2.3	−26.7 ± 3.4
γS-C_0	0.84 ± 0.15	6.2 (± 1.2) × 10^6	−10.3 ± 1.2	−29.8 ± 0.5	−19.5 ± 0.4